The signaling lipid sphingosine 1-phosphate regulates mechanical pain

Authors and Affiliations: Rose Z. Hill[1], Benjamin U. Hoffman[2, 3], Takeshi Morita[1#], Stephanie M. Campos[4‡], Ellen A. Lumpkin[2, 4], Rachel B. Brem[5, 6], Diana M. Bautista[1, 4, 7, 8*]

1. Department of Molecular and Cell Biology, University of California, Berkeley, CA 94720, USA.
2. Department of Physiology & Cellular Biophysics, Columbia University College of Physicians & Surgeons, New York, NY 10032
3. Medical Scientist Training Program, Columbia University, New York, NY 10032
4. Neurobiology Course, Marine Biological Laboratory, Woods Hole, MA
5. Department of Plant and Microbial Biology, University of California, Berkeley, CA 94720, USA.
6. Buck Institute for Research on Aging, Novato, CA 94945, USA.
7. Helen Wills Neuroscience Institute, University of California, Berkeley, CA 94720, USA.
8. Corresponding author

[#] Current Address: Rockefeller University, New York, NY 10065, USA.

[‡] Current Address: Indiana University, Bloomington, IN 47405, USA.

* Correspondence: dbautista@berkeley.edu

Abstract

Somatosensory neurons mediate responses to diverse mechanical stimuli, from innocuous touch to noxious pain. While recent studies have identified distinct populations of A mechanonociceptors (AMs) that are required for mechanical pain, the molecular underpinnings of mechanonociception remain unknown. Here, we show that the bioactive lipid sphingosine 1-phosphate (S1P) and S1P Receptor 3 (S1PR3) are critical regulators of acute mechanonociception. Genetic or pharmacological ablation of S1PR3, or blockade of S1P production, significantly impaired the behavioral response to noxious mechanical stimuli, with no effect on responses to innocuous touch or thermal stimuli. These effects are mediated by fast-conducting A mechanonociceptors, which displayed a significant decrease in mechanosensitivity in S1PR3 mutant mice. We show that S1PR3 signaling tunes mechanonociceptor excitability via modulation of KCNQ2/3 channels. Our findings define a new role for S1PR3 in regulating neuronal excitability and establish the importance of S1P/S1PR3 signaling in the setting of mechanical pain thresholds.

Introduction

Pain is a complex sensation. It serves to protect organisms from harmful stimuli, but can also become chronic and debilitating following tissue injury and disease. Distinct cells and molecules detect noxious thermal and mechanical stimuli. Thermal pain is detected by thermosensitive TRP channels in subsets of nociceptors[1,2], and gentle touch is detected by Piezo2 channels in low-threshold mechanoreceptors (LTMRs)[3,4]. Aδ high-threshold mechanoreceptors (HTMRs) have been shown to play a key role in responses to painful mechanical stimuli[5,6].

Recent studies have shown that there are at least two populations of HTMRs that mediate responses to noxious mechanical stimuli. The *Npy2r*$^{+}$ subpopulation of HTMRs mediates fast paw withdrawal responses to pinprick stimulation and terminates as free nerve endings in the epidermis[5]. The *Calca*$^{+}$ subpopulation of circumferential-HTMRs responds to noxious force and hair pulling, and terminates as circumferential endings wrapped around guard hair follicles[6]. Additionally, somatostatin-expressing interneurons of laminae I-III in the dorsal horn of the spinal cord receive input from nociceptors and are required for

77 behavioral responses to painful mechanical stimuli[7]. Despite these advances in defining the cells and
78 circuits of mechanical pain, little is known about the molecular signaling pathways in mechanonociceptors.
79
80 Here, we show that sphingosine 1-phosphate (S1P) is required for mechanical pain sensation. S1P is a
81 bioactive lipid that signals via 5 G-protein coupled S1P Receptors (S1PRs 1-5). S1P signaling, mainly via
82 S1PR1, plays a well-known role in immune cell migration and maturation[8–10]. Additionally, recent studies
83 have shown that S1PRs are expressed throughout the nervous system[11–13] and S1P signaling is associated
84 with a variety of neuroinflammatory disorders, including multiple sclerosis[14] and Alzheimer's disease[15]. S1P
85 has been implicated in spontaneous pain[13] and thermal pain hypersensitivity[12,16,17], but due to conflicting
86 accounts of S1P receptor expression in the CNS[11,18] and PNS[12,13,19] as well as inconsistent reports on the
87 effects of S1P on neuronal excitability[13,20,21] and pain behaviors[12,13,16,17], the role of S1P in somatosensation
88 remains controversial.
89
90 We found that mice lacking the S1P receptor S1PR3 display striking and selective deficits in behavioral
91 responses to noxious mechanical stimuli. Likewise, peripheral blockade of S1PR3 signaling or S1P
92 production impairs mechanical sensitivity. We found that S1P constitutively enhances the excitability of
93 A mechanonociceptors (AMs) via closure of KCNQ2/3 potassium channels to tune mechanical pain
94 sensitivity. The effects of S1P are completely dependent on S1PR3. While previous studies have shown
95 that elevated S1P triggers acute pain and injury-evoked thermal sensitization[12,13], we now show that
96 baseline levels of S1P are necessary and sufficient for setting normal mechanical pain thresholds. In
97 contrast, elevated S1P selectively triggers thermal sensitization via activation of TRPV1^{+} heat nociceptors,
98 with no effect on mechanical hypersensitivity. Our findings uncover an essential role for constitutive S1P
99 signaling in mechanical pain.
100

101 Results

102 To identify candidate genes underlying mechanosensation, we previously performed transcriptome
103 analysis of the sensory ganglia innervating the ultra-sensitive tactile organ (the star) of the star-nosed
104 mole[22]. Immunostaining revealed the tactile organ is preferentially innervated by myelinated Aδ fibers[22],

105 which are primarily mechanosensitive. While our original analysis focused on ion channels enriched in the
106 neurons of the star organ, our dataset also revealed enrichment of several components of the S1P
107 pathway, including *S1pr3*. Likewise, single-cell RNA seq of mouse dorsal root ganglion (DRG) neurons
108 revealed *S1pr3* expression in a subset of myelinated mechanoreceptors[19] in addition to a subpopulation of
109 peptidergic C nociceptors.
110
111 S1P promotes excitability in small-diameter, capsaicin-sensitive nociceptors[12,13,20,21]. In addition, S1PR3
112 has been shown to mediate spontaneous pain triggered by elevated S1P and thermal sensitization
113 following sterile tissue injury[13]. However, no studies have examined the role of S1PR3 in
114 mechanosensation or in regulating somatosensory behaviors under normal conditions. Given the
115 enrichment of S1PR3 in specialized mechanosensory neurons of the star-nosed mole and mouse, we
116 hypothesized that S1P signaling via S1PR3 may also play a role in mechanosensation. Thus, we set out to
117 define the role of S1P signaling and S1PR3 in somatosensory mechanoreceptors.
118
119 **S1PR3 mediates acute mechanical pain**
120 We first examined a variety of somatosensory behaviors in mice lacking S1PR3[23] (*S1pr3*$^{tm1Rlp/Mmnc}$; referred
121 to herein as S1PR3 KO). We initially investigated baseline responses to mechanical stimuli. S1PR3 KO
122 mice displayed a dramatic loss of mechanical sensitivity (**Figure 1A; see Figure 1-source data 1**), as von
123 Frey paw withdrawal thresholds were significantly elevated in S1PR3 KO mice relative to WT and S1PR3
124 HET littermates (mean thresholds: 1.737 g vs. 0.736 and 0.610 g, respectively). Moreover, S1PR3 KO
125 mice demonstrated decreased responses to a range of noxious tactile stimuli (2-6 g; **Figure 1B**) and to
126 noxious pinprick stimulation (**Figure 1C**), but normal responsiveness to innocuous tactile stimuli (0.6-1.4g;
127 **Figure 1B**). S1PR3 KO mice exhibited normal tape removal attempts[3] (**Figure 1D**), righting reflexes
128 (**Figure 1-figure supplement 1A**), radiant heat withdrawal latencies (**Figure 1E**), and itch-evoked
129 scratching (**Figure 1-figure supplement 1B**). These results demonstrate a selective role for S1PR3 in
130 acute mechanical pain.
131
132 As a complement to our analysis of somatosensation in S1PR3 KO animals, we employed a

133 pharmacological approach, using the S1PR3-selective antagonist TY 52156 (TY)[24]. Similar to the
134 phenotype of knockout animals, intradermal injection of 500 μM TY into the mouse hindpaw (the site of
135 testing) triggered a rapid and significant elevation in von Frey paw withdrawal thresholds (**Figure 1F**) and
136 decreased responsiveness to noxious (2-6 g), but not innocuous (0.6-1.4g), tactile stimuli (**Figure 1G**),
137 without affecting noxious heat sensitivity (**Figure 1-figure supplement 1C**). In contrast, blockade of
138 S1PR1 with the selective antagonist W146[16] had no effect on baseline mechanical or thermal thresholds
139 (**Figure 1F; Figure 1-figure supplement 1C**). Overall, these data show that S1PR3 signaling sets
140 mechanical pain sensitivity.
141
142 **Endogenous S1P mediates acute mechanical pain**
143 We next asked whether peripheral S1P was required for the S1PR3-dependent effects on
144 mechanosensation. We decreased S1P levels via injection of the sphingosine kinase inhibitor SKI II to
145 block local production of S1P[25] or elevated S1P levels via intradermal injection of S1P and measured
146 behaviors 30 minutes after injection. Decreasing local S1P levels with SKI II significantly reduced
147 mechanical sensitivity (**Figure 2A; see Figure 2-source data 1**), comparable to the hyposensitivity
148 phenotype observed in S1PR3 KO mice (**Figure 1A**). Again, similar to what was observed in S1PR3 KO
149 animals (**Figure 1E**), peripheral blockade of S1P production had no effect on baseline thermal sensitivity
150 (**Figure 1-figure supplement 1C**). Surprisingly, injecting exogenous S1P (10 μM; maximum solubility in
151 saline vehicle) had no effect on mechanical sensitivity (**Figure 2A-B**). However, as previously reported[12,13],
152 S1P injection triggered S1PR3-dependent thermal hypersensitivity and spontaneous pain (**Figure 2C-D**),
153 demonstrating that the lack of effect on mechanical hypersensitivity is not due to problems with S1P
154 delivery or degradation.
155
156 These data support a model whereby S1P constitutively activates S1PR3 to set normal mechanical pain
157 thresholds. To further test this model, we asked if the mechanical hyposensitivity elicited after endogenous
158 S1P depletion (via SKI II) could be rescued by local injection of exogenous S1P. Indeed, we found that
159 injection of exogenous S1P reversed SKI II-induced mechanical hyposensitivity in a dose-dependent
160 manner, and observed a maximal effect with 200 nM S1P (**Figure 2E**). Although quantification of native

161 S1P levels in skin is inaccurate owing to avid lyase activity[26], our data establish that baseline S1P levels
162 are sufficient to maximally exert their effect on S1PR3-dependent mechanical pain, such that increased of
163 S1P does not evoke mechanical hypersensitivity, but diminished S1P leads to mechanical hyposensitivity.
164 These data show that constitutive activation of S1PR3 by S1P is required for normal mechanosensitivity.
165

166 **S1PR3 is expressed in A mechanonociceptors and thermal nociceptors**

167 Our behavioral data showing distinct roles for S1PR3 in mechanonociception and thermal hypersensitivity
168 suggest that S1PR3 is expressed in distinct subsets of somatosensory neurons. While a previous study
169 suggested that all somatosensory neurons express S1PR3[13], single cell RNA seq data suggests *S1pr3* is
170 not expressed by all DRG neurons[19], and no studies have performed quantitative analysis of S1PR3
171 staining or co-staining to define subpopulations of S1PR3^{+} neurons. We thus set out to characterize the
172 somatosensory neuron subtypes expressing *S1pr3* using *in situ* hybridization (ISH) of wild-type
173 somatosensory ganglia and immunohistochemistry (IHC) in an *S1pr3*$^{mCherry/+}$ reporter mouse[27].
174

175 We first used *in situ* hybridization (ISH) with a specific *S1pr3* probe to examine expression patterns of
176 *S1pr3* (**Figure 3A-B**; see **Supplementary File 1**). In our experiments, 43% of cells from wild-type DRG
177 expressed *S1pr3*. Co-ISH revealed that one population of *S1pr3*$^{+}$ neurons represents Aδ
178 mechanonociceptors (AMs). These cells expressed *Scn1a* (39.9% of all *S1pr3*$^{+}$), a gene that encodes the
179 Nav1.1 sodium channel, which mediates mechanical pain in Aδ fibers[28]. *S1pr3*$^{+}$ cells also co-expressed
180 *Npy2r* (20.4% of all *S1pr3*$^{+}$), a marker of a subset of mechanonociceptive A fibers[5]. *S1pr3* was expressed
181 in 70.6% of *Scn1a*$^{+}$ cells and 72% of *Npy2r*$^{+}$ cells, comprising a majority of both of these populations.
182 Interestingly, a subset of cells co-expressed *S1pr3* and the mechanically sensitive channel *Piezo2*, which is
183 expressed by Aβ, Aδ, and C fibers[3]. The remaining *S1pr3*$^{+}$ cells were *Trpv1*$^{+}$ and/or *Trpa1*$^{+}$ C nociceptors
184 (67.1% of all *S1pr3*$^{+}$), which are reported to overlap minimally with the *Scn1a*$^{+}$ and *Npy2r*$^{+}$ populations[5,28].
185

186 We next used an *S1pr3*$^{mCherry/+}$ reporter mouse, which produces a functional S1PR3-mCherry fusion
187 protein[27], as an independent strategy to explore S1PR3 expression and localization. This strategy was
188 used because we found that anti-S1PR3 antibodies showed broad immunoreactivity in DRG from mice
189 lacking S1PR3, and so we instead used anti-DsRed antibodies to probe expression of the S1PR3 fusion

190 protein (**Figure 3-figure supplement 1E**). We found that 42.4% S1PR3$^+$ cells co-stained with anti-
191 Peripherin, demonstrating that S1PR3 is expressed in a subset of small-diameter neurons. We also
192 observed that 69.5% of S1PR3$^+$ cells co-stained with anti-NF200, which marks medium and large-diameter
193 myelinated neurons. Furthermore, we observed that S1PR3$^+$ cells were primarily of small to medium
194 diameter (11.3-35.1 μm), whereas all cells in the DRG ranged from 11.3-53.9 μm. Overall, these data
195 support the expression of S1PR3 in subsets of small-diameter thermal nociceptors and medium-diameter
196 mechanonociceptors (**Figure 3F**). Additionally, no significant differences were observed between WT and
197 S1PR3 KO DRG in number of *Trpa1, Trpv1,* Peripherin-, NF200-, or IB4-positive cells (**Figure 3-figure**
198 **supplement 1B-C, F, G**). The mean diameters of *Trpv1*$^+$ neurons (**Figure 3-figure supplement 1D**, left),
199 NF200$^+$ neurons (**Figure 3-figure supplement 1G**), or all neurons (**Figure 3-figure supplement 1D**, right)
200 in WT versus KO DRG were not significantly different, suggesting no loss of major sensory neuronal
201 subtypes in the S1PR3 KO.
202
203 We then visualized S1PR3 expression in nerve fibers that innervate the skin using anti-DsRed antibodies in
204 whole-mount immunohistochemistry (IHC; **Figure 3D**). The reporter animals showed no specific antibody
205 staining in epidermal or dermal cells (**Figure 3-figure supplement 1I**), and single-cell RNA seq of a
206 diverse array of mouse epidermal and dermal cells corroborates this lack of expression[29]. We observed
207 overlap of S1PR3-expressing free nerve endings with NF200-positive myelinated free nerves and NF200-
208 negative putative C-fiber endings (**Figure 3F**), but did not observe expression of S1PR3 in NF200-positive
209 circumferential or lanceolate hair follicle receptors, or in putative Merkel afferents (**Figure 3D-E**). β-tubulin
210 III, PGP9.5 (pan-neuronal markers), and NF200 staining in S1PR3 KO skin displayed patterns of epidermal
211 and dermal innervation similar to WT skin, suggesting the phenotypes observed in the S1PR3 KO mice are
212 not due to developmental loss of sensory neuronal innervation ($p_{PGP9.5}$ = 0.443 (n = 93, 38 fibers); p_{NefH} =
213 0.405 (n = 61, 28 fibers); p_{BTIII} = 0.353 (n = 104, 89 fibers); two-tailed t-tests based on average number of
214 fibers per field of view). These results support expression of S1PR3 in subsets of myelinated A
215 mechanonociceptors and unmyelinated C nociceptors that terminate as free nerve endings.
216
217

218 **S1P activates thermal nociceptors but not putative AMs**

219 Live imaging of cultured DRG neurons from adult reporter animals showed expression of S1PR3-mCherry
220 fusion protein in 48.3% of neurons, mirroring our ISH and IHC results (**Figure 4A**). To examine the effects
221 of S1P on A mechanonociceptors and C nociceptors, we performed ratiometric calcium imaging and
222 electrophysiology on DRG cultures from reporter mice. Interestingly, only 56.1 ± 22.4 % of mCherry-
223 expressing neurons were activated by 1 μM S1P (Representative trace in **Figure 4B**; representative
224 images in **Figure 4C**), which our dose-response showed to be the saturating concentration for calcium
225 influx (**Figure 4D**; EC_{50} = 155 nM). All S1P-responsive neurons were also capsaicin-sensitive (n > 2000
226 neurons). And while sensory neurons from S1PR3 KO animals did not respond to S1P, as expected[13], they
227 exhibited capsaicin responses that were not significantly different from WT neurons (**Figure 3-figure**
228 **supplement 1H**). The mean diameter of S1P-responsive $mCherry^+$ neurons was 22.4 ± 1.0 μm, whereas
229 the mean diameter of non-responsive $mCherry^+$ neurons was 28.7 ± 3.2 μm (p = 0.0002, two-tailed t-test).
230 We also performed whole cell current clamp experiments and, consistent with other studies[12,20,21], found
231 that S1P evoked action potential firing in capsaicin-sensitive small diameter cells (**Figure 4E**). This shows
232 that only the small-diameter, $S1PR3^+$ putative nociceptors are excited by S1P. We next asked whether the
233 $S1PR3^+$ medium-large diameter neurons represent the mechanonociceptors observed by ISH (**Figure 3A**).
234 To this end, we asked whether the spider toxin Hm1a, a selective activator of AM nociceptors[28], triggers
235 calcium influx in S1PR3-expressing trigeminal neurons. Indeed, we found that 44.2 ± 15.1% of Hm1a-
236 responsive neurons expressed mCherry (**Figure 4F**), consistent with our staining showing expression of
237 *S1pr3* in AM nociceptors and the role of Hm1a-responsive neurons in mediating mechanical pain *in vivo*[28].

238

239 **S1PR3 modulates KCNQ2/3 channels to regulate AM excitability**

240 We next interrogated the molecular mechanism by which S1P signaling in AM nociceptors may regulate
241 mechanical pain. We performed whole-cell current clamp on the medium-diameter $S1pr3^{mCherry/+}$ dissociated
242 DRG neurons (membrane capacitance = 61.05 ± 1.92 pF), which did not display S1P-evoked calcium influx
243 (**Figure 4B-C**). In these cells, 1 μM S1P application did not change membrane potential (**Figure 5-figure**
244 **supplement 1A;** see **Figure 5-source data 1**) or elicit firing in the absence of current injection (**Figure 5-**
245 **figure supplement 1A**; **Figure 5A**). However, S1P dramatically lowered the threshold to fire action

246 potentials (rheobase) in an S1PR3-dependent manner (**Figure 5A**, **Figure 5-figure supplement 1B**).

247

248 We then set out to determine the mechanism by which S1PR3 activity increases neuronal excitability using
249 whole-cell voltage clamp recording. Previous studies showed that S1P excites capsaicin-sensitive
250 nociceptors by increasing voltage-gated sodium currents and reducing steady-state potassium currents[20,21].
251 We found that S1P had no such effects on S1PR3^{+} medium-diameter cells (**Figure 5-figure supplement**
252 **1C-F**). In contrast, S1P triggered a robust increase in input resistance (**Figure 5B**), consistent with the
253 closure of potassium channels. I-V analysis revealed that the current inhibited by S1P application was
254 carried by potassium (**Figure 5C**). Additionally, S1P significantly reduced slow, voltage-dependent tail
255 current amplitudes (**Figure 5D**; **Figure 5E** (top)) in an S1PR3-dependent manner (**Figure 5D**, center).

256

257 As tail currents in Aδ neurons are primarily mediated by KCNQ2/3 potassium channels[30,31], we postulated
258 that S1P may alter tail currents through modulation of these channels. Furthermore, the above properties
259 of the S1P-sensitive current were consistent with the reported electrophysiological properties of KCNQ2/3
260 channels in DRG neurons[30,32,33]. To address whether KCNQ2/3 channels mediated S1P-dependent
261 neuronal excitability, we applied the KCNQ2/3-selective inhibitor XE 991 and found that it completely
262 occluded the effects of S1P on tail current (**Figure 5E**). Similar results were observed with the related
263 antagonist, linopirdine (**Figure 5E**). These findings are consistent with S1P/S1PR3-dependent inhibition of
264 KCNQ2/3 in somatosensory neurons.

265

266 We also found that the effect of S1P on KCNQ2/3 currents was mediated by low levels of S1P, exhibiting
267 an IC_{50} of 48 nM with saturation at 100 nM (**Figure 5-figure supplement 1F**). While S1P cannot be
268 accurately measured in non-plasma tissues, this is similar to estimated levels of S1P in peripheral
269 tissues[10,34], and to levels which were sufficient to rescue mechanosensitivity after local S1P depletion
270 (**Figure 2E**). Thus, our *in vitro* IC_{50} supports our behavioral observations that baseline S1P levels are
271 sufficient to maximally exert their effect on mechanical pain. In summary, our electrophysiological and
272 behavioral observations support a model in which baseline S1P/S1PR3 signaling governs mechanical pain
273 thresholds through modulation of KCNQ2/3 channel activity in AM neurons (**Figure 8**).

274 **S1PR3 is required for nociceptive responses of high-threshold AM nociceptors**

275 Given the effects of S1P on putative AM neurons *in vitro* and the selective attenuation of baseline
276 mechanical pain in S1PR3 KO animals, we hypothesized that S1PR3 would play a role in AM afferent
277 function. To test this, we utilized *ex vivo* skin-nerve recordings to analyze the effects of genetic ablation of
278 S1PR3 on AM afferents, which mediate fast mechanical pain sensation. As no significant differences were
279 observed between S1PR3 WT and S1PR3 HET mice in any behavioral assays (**Figure 1**) or in AM force-
280 response relationships[28,35–38] (**Figure 6-figure supplement 1A;** see **Figure 6-source data 1**), we
281 compared AM nociceptor function between S1PR3 HET and S1PR3 KO littermates. S1PR3 KO AM
282 nociceptors displayed reduced sensitivity in their force-response relation (slope for HET versus KO: 50
283 Hz/N versus 35 Hz/N), as well as attenuated firing over the noxious, but not innocuous, range of
284 mechanical stimulation (**Figure 6A**). Strikingly, the median von Frey threshold to elicit firing in AM
285 nociceptors was significantly higher in S1PR3 KO animals (3.92 mN) compared to littermate controls (1.56
286 mN; **Figure 6B**).

287

288 Furthermore, S1PR3 KO AM nociceptors displayed a right-shifted cumulative response curve (50%
289 effective force for HET versus KO: 33.7 versus 60.0 mN; **Figure 6C**), consistent with the
290 mechanonociceptive hyposensitivity observed *in vivo*. A recent report suggested that A-nociceptors are
291 composed of two distinct neuronal populations that differ genetically, in mechanically evoked response
292 patterns, and in conduction velocity[5]. Accordingly, we found in the S1PR3 KO that a proportion of "Adapting
293 AM" nociceptors, characterized by adapting responses to static mechanical stimuli, were unresponsive to
294 controlled force stimulation (**Figure 6E-F**), and only responded to stimulation with a blunt glass probe or to
295 suprathreshold stimulation with von Frey filaments (see Methods). However, we found no differences in
296 conduction velocity between genotypes (**Figure 6D**) or the proportions of Aβ, Aδ, and C fibers between
297 wild-type and KO animals (**Figure 6-figure supplement 1B**). We conclude that S1PR3 is an essential
298 regulator of both mechanical threshold and sensitivity in a distinct population of AM nociceptors.

299

300

301

302 **S1PR3 is required for inflammatory pain hypersensitivity**

303 Having examined the mechanisms of S1P/S1PR3 signaling in acute mechanonociception, we next sought
304 to evaluate S1P/S1PR3 signaling in pain hypersensitivity. For this purpose, we used an experimental
305 model of inflammatory pain triggered by Complete Freund's Adjuvant (CFA) injection into the hindpaw,
306 which elicits infiltration of immune cells and thermal and mechanical hypersensitivity[39]. While one previous
307 study proposed that S1PR3 promotes injury-evoked heat and mechanical hypersensitivity, they did not
308 measure or compare post-injury mechanical thresholds to pre-injury baselines for the knockout or control
309 animals[13]. Here, we compared development of CFA-evoked hypersensitivity between S1PR3 HET and KO
310 littermates, since no significant behavioral differences were observed between WT and HET animals in
311 CFA experiments ($p_{\text{von Frey}}$ = 0.12; $p_{\text{radiant heat}}$ = 0.12; two-tailed *t*-tests). Strikingly, S1PR3 KO mice failed to
312 develop thermal hypersensitivity (**Figure 7A;** see **Figure 7-source data 1**) relative to heterozygous
313 littermates at both 24 and 48 hours post-CFA injection. In stark contrast, S1PR3 KO animals developed
314 robust mechanical hypersensitivity when thresholds were normalized to account for the dramatic baseline
315 differences between knockouts and control animals (**Figure 7B**). Our data demonstrate that S1PR3
316 mediates baseline mechanical sensitivity and is not required for the development of CFA-evoked
317 mechanical hypersensitivity.

318

319 Influx of myeloid lineage ($Cd11b^+/Ly6G^-$) cells is required for the development of mechanical
320 hypersensitivity in the CFA model[39]. In the immune system, S1P signaling via S1PR1 plays a key role in
321 immune cell migration[9]. Consistent with the development of mechanical hypersensitivity, flow cytometry
322 experiments showed robust infiltration of immune cells into hindpaw skin from both S1PR3 KO and
323 littermate controls (**Figure 7-figure supplement 1A-B**). These data suggest that the phenotypes observed
324 in S1PR3 KO mice cannot be attributed to compromised immune cell infiltration.

325

326 Next, we tested whether active S1P/S1PR3 signaling was required to maintain CFA-evoked thermal
327 hypersensitivity using pharmacology. Acute blockade of S1P production with SKI II or S1PR3 with TY also
328 reversed CFA heat hypersensitivity (**Figure 7C**), demonstrating that peripheral S1P actively signals via
329 S1PR3 to promote CFA-evoked heat hypersensitivity. Furthermore, acute S1P/S1PR3 blockade with SKI II

330 or TY elevated mechanical thresholds to pre-CFA, baseline levels (**Figure 7D**) showing that S1PR3 tunes
331 mechanical pain under normal and inflammatory conditions. These results are consistent with the distinct
332 roles for AM and C nociceptors in mechanical pain. Under normal conditions, AM nociceptors set
333 mechanical pain thresholds[28,40]. In contrast, under inflammatory conditions, the combined activity of both
334 non-sensitized AM fibers and sensitized C fibers determines overall post-inflammatory mechanical
335 thresholds[41,40]. Consistent with this model, acute blockade of S1P production or S1PR3 activity under
336 normal conditions induces mechanical hyposensitivity and under inflammatory conditions returns
337 mechanical sensitivity to normal levels.
338

339 Discussion

340 We now show that S1P signaling via S1PR3 is a key pathway that tunes mechanical pain sensitivity.
341 Overall, our data reveal two new key findings. First, S1P/S1PR3 sets baseline mechanical pain thresholds.
342 Depletion of baseline, endogenous S1P induces mechanical hyposensitivity and nanomolar levels of
343 exogenous S1P are sufficient to restore normal mechanical pain sensitivity after depletion. Second,
344 elevated micromolar S1P levels, such as those produced during inflammation or disease, promote thermal,
345 but not mechanical hypersensitivity. The effects of S1P on acute mechanical pain and thermal
346 hypersensitivity are completely lost in S1PR3 knockout animals, which are otherwise normal with respect to
347 other somatosensory behaviors.
348

349 What is the local source of S1P in the skin that constitutively modulates mechanical pain? Even in the
350 mature field of S1P signaling in the vascular and immune systems, the cellular source of S1P, while an
351 intriguing question, remains unclear. All cells in the body, including somatosensory neurons, immune cells,
352 and skin cells, express sphingosine kinases 1 and 2 which are essential for S1P production[42]. Deletion of
353 both kinases is lethal and attempts to conditionally knockout these kinases fail to completely eliminate S1P
354 in tissues[43]. While RNA seq data suggests that somatosensory neurons contain all of the enzymatic
355 machinery required to produce and export local S1P[19,44], future work will be needed to identify the key cell
356 types that are important for maintaining baseline S1P levels in the skin to regulate mechanical sensitivity
357 and for increasing S1P under inflammatory/injury conditions to promote pain hypersensitivity.

358

359 Recent studies have identified distinct populations of AM nociceptors that are required for mechanical
360 pain[5,6]. Likewise, it was discovered that a subset of somatostatin-expressing spinal interneurons is required
361 for mechanical pain transduction[7]. Although these papers delineate the cells and circuitry of mechanical
362 pain, the molecular underpinnings of mechanonociception in the periphery are poorly understood. While
363 the identity of the transduction channel(s) in AM nociceptors remains enigmatic, understanding molecular
364 mechanisms that regulate excitability will no doubt provide key insights into the function and specialization
365 of the diverse subtypes of mechanosensitive nerve fibers. For example, although *Piezo2*-hypomorphic
366 animals exhibit normal mechanical pain behaviors[3], *ex vivo* skin-nerve recordings show that their AM
367 nociceptors display decreased force-responsiveness[3], and a recent study found that subpopulations of
368 sensory neurons express different splice variants of *Piezo2* that exhibit different force sensitivities[45]. These
369 studies suggest that mechanosensitive neurons exhibit functional specialization on multiple levels. Our
370 study demonstrates that S1PR3 is indispensable for normal function of AM nociceptors, including the
371 adapting AM population, recently discussed in Arcourt *et al.,* that innervates the epidermis and encodes
372 noxious touch[5]. We show that S1PR3 signaling modulates KCNQ2/3 channels to regulate excitability of
373 these A mechanonociceptors (**Figure 8**).

374

375 GPCR-mediated inhibition of KCNQ2/3 potassium channels is a well-known mechanism by which neuronal
376 excitability is regulated[46]. Other studies have shown that KCNQ channels mediate excitability of Aδ
377 fibers[30,31] and are required for normal mechanonociceptive responses in dorsal horn neurons receiving Aδ
378 input[31], and that opening KCNQ2/3 channels directly with retigabine alleviates pain *in vivo*[33,47,48]. Our
379 results not only complement previous work implicating KCNQ2/3 channels in pain, but also define the
380 upstream mechanisms that promote the regulation of KCNQ2/3 channels to tune mechanical pain
381 thresholds. Our data thus highlight S1PR3 as a novel and attractive target for the treatment of mechanical
382 pain and describe a new signaling pathway by which S1P regulates AM nociceptor excitability.

383

384 Interestingly, the neurons that innervate the ultra-sensitive tactile organ of the star-nosed mole are highly
385 enriched in transcripts for S1PR3 and KCNQ channels, as well as for a variety of other potassium

386 channels[22]. While it is difficult to directly examine the physiological basis for heightened mechanosensitivity
387 in the star-nosed mole, S1PR3-dependent modulation of KCNQ may represent an important mechanism
388 underlying the high tactile sensitivity of the star organ. Moreover, link between *S1pr3* and *Kcnq2/3* are
389 echoed in single-cell RNA seq datasets from mouse DRG neurons, which show co-expression of *S1pr3*
390 and *Kcnq2/3* in a subset of myelinated mechanoreceptors[19]. These cells are distinct from the *S1pr3/Trpv1*
391 subset that mediates S1P-evoked acute pain and heat hypersensitivity. In addition to being transcriptionally
392 distinct, we show that the mechanisms underlying S1P's activities in these cells are functionally distinct.
393 Finally, *S1pr3* and *Kcnq2/3* are highly expressed in human sensory ganglia[49,50] and recordings from human
394 stem cell-derived sensory neurons show that KCNQ2/3 channels play a key role in mediating their
395 excitability[51]. Thus S1PR3 signaling may represent a new target for modulating mechanical pain.
396
397 Previous studies of S1P signaling in DRG neurons focused on S1P-evoked excitation of small diameter
398 and/or capsaicin-sensitive neurons, and pain behaviors triggered by elevated S1P. While our new data
399 affirms the effects S1P in thermal nociceptors observed by others, our manuscript highlights a novel effect
400 of baseline levels of S1P in modulation of rheobase and KCNQ2/3 currents in mechanonociceptors. We
401 are also the first to examine the role of S1PR3 in a variety of somatosensory behaviors under normal
402 conditions (non-injury, no algogen injection), and to demonstrate a key role for S1PR3 in
403 mechanonociception. We also go beyond previous studies[12,13,16,17] in showing that elevated S1P
404 selectively promotes thermal and not mechanical hypersensitivity. Previous studies have shown that there
405 are distinct cells and molecular pathways that trigger thermal versus mechanical hypersensitivity. For
406 example, thermal hypersensitivity in CFA is dependent on TRPV1 ion channels[1] and independent of
407 immune cell infiltration[39]. In contrast, infiltration of a subset of myeloid immune cells is required for
408 mechanical hypersensitivity in an inflammatory pain model[39]. Here we show that S1P via S1PR3 signaling
409 is a key component of the inflammatory soup that triggers thermal hypersensitivity in the CFA model. Our
410 observation that S1PR3 KO animals display normal immune cell infiltration and develop mechanical
411 hypersensitivity after CFA is consistent with these previous studies showing distinct mechanisms of
412 inflammatory thermal and mechanical hypersensitivity.
413

414 Outside of the nervous system, S1P signaling via S1PR1 allows for the continuous circulation of
415 lymphocytes between blood, lymph, and peripheral tissues[9]. Our findings that S1P plays a key role in
416 noxious mechanosensation are in line with recent studies showing that sensory neurons co-opt classical
417 immune pathways to drive chronic itch or pain[52,53]. What distinguishes this study from the others is that S1P
418 signaling is critical for acute mechanical pain, even in the absence of inflammation or exogenously elevated
419 S1P. In the immune system, disruptions in S1P levels or S1PR1 signaling result in significant immune
420 dysfunction and disease[54–56]. Accordingly, in the somatosensory system, excessive, high levels of S1P
421 (micromolar), such as those present in inflammation, evokes thermal pain and sensitization. Intermediate,
422 baseline levels (nanomolar) regulate AM excitability and are required for normal mechanical pain
423 sensation. In contrast, lowering S1P levels reduces mechanical pain sensation, while sparing innocuous
424 touch sensation.
425
426 We propose that S1PR3 signaling may contribute to a variety of inflammatory diseases. S1P has been
427 linked to a wide range of human inflammatory disorders[57–63]. Canonically, S1P signaling via S1PR1 is
428 thought to promote inflammation via the immune system[58], however, we propose that S1P signaling via
429 S1PR3 in neurons may also contribute to inflammatory disease. Indeed, fingolimod, a non-selective S1PR
430 modulator, is prescribed as an immunosuppressant for multiple sclerosis treatment[14], but the possibility that
431 some of its therapeutic effects may also be mediated via the nervous system has not been fully explored.
432 Likewise, one study found that intrathecal fingolimod reduces bone cancer pain[64], and while analgesia was
433 attributed to effects on S1PR1 in glia, some of the benefits may be due to S1PR3 signaling in DRG
434 neurons. S1PR3 antagonism may also be useful in the treatment of inflammatory pain due to its selective
435 dampening of acute mechanical pain and inflammatory thermal hypersensitivity, while preserving
436 innocuous touch and normal thermal sensitivity. S1PR3 inhibitors may also be beneficial for treating other
437 inflammatory disorders where S1PR3-expressing somatosensory neurons have been shown to contribute
438 to neurogenic inflammation, such as asthma[65]. Our study demonstrates a crucial role for S1P signaling in
439 the peripheral nervous system and highlights the potential of S1PR3 as a target for future pain therapies.
440
441

442 # Materials and Methods

443 *Behavioral studies & mice*

444 *S1pr3*$^{mcherry/+}$ and *S1pr3*$^{-/-}$ mice were obtained from Jackson Laboratory and backcrossed to C57bl6/J.
445 Wherever possible, wild-type/heterozygous (*S1pr3)* littermate controls were used in behavioral
446 experiments. Mice (20–25 g) were housed in 12 h light-dark cycle at 21°C. Mice were singly housed one
447 week prior to all behavioral experiments and were between 8-10 weeks at the time of the experiment. All
448 mice were acclimated in behavioral chambers (IITC Life Sciences) on 2 subsequent days for 1 hour prior to
449 all behavioral experiments.

450

451 Itch and acute pain behavioral measurements were performed as previously described[44,66,67]. Mice were
452 shaved one week prior to itch behavior. Compounds injected: 500 μM TY 52156 (Tocris), 50 μM SKI II
453 (Tocris), 0.2-10 μM S1P (Tocris, Avanti Polar Lipids), 50 mM chloroquine (Sigma), and 27 mM histamine
454 (Tocris) in PBS with either 0.01-0.1% Methanol- (S1P) or 0.1-0.5% DMSO-PBS (all other compounds)
455 vehicle controls. Pruritogens were injected using the cheek model (20 μL) of itch, as previously described[68].
456 Behavioral scoring was performed while blind to experimental condition and mouse genotype. All
457 scratching and wiping behavior videos were recorded for 1 hour. Itch behavior was scored for the first 30
458 minutes and acute pain was scored for the first five minutes. Bout number and length were recorded.

459

460 For radiant heat and von Frey hypersensitivity behavior, drugs were injected intradermally into the plantar
461 surface of the hindpaw (20 μL). Radiant heat assays were performed using the IITC Life Science
462 Hargreaves test system. Mechanical threshold was measured using calibrated von Frey monofilaments
463 (Touch Test) on a metal grate platform (IITC). Von Frey was performed as previously described[67,69] using
464 the up-down method[70] while blinded to compound injected and genotype, or a descending force-series of 4
465 trials per force from 0.4 g to 6 g. Valid responses for both von Frey and radiant heat included fast paw
466 withdrawal, licking/biting/shaking of the affected paw, or flinching. For radiant heat and von Frey, mice were
467 allowed to acclimate on platform for 1 hour before injection. Measurements were taken 15 minutes pre-
468 injection and 20-30 minutes post-injection for all compounds used.

469

470 The pinprick assay[7] was conducted on a von Frey testing platform (IITC). The mouse hindpaw was poked
471 with a 31 g syringe needle without breaking the skin to induce fast acute mechanical pain. Each paw was
472 stimulated 10 times with the needle, with five minutes rest in between trials, and the % withdrawal (fast
473 withdrawal, licking/biting/shaking of paw, squeaking, and/or flinching) was calculated from the total number
474 of trials.
475
476 The tape assay was conducted according to previously described methods[3]. Number of attempts to remove
477 a 3 cm piece of lab tape was recorded for 10 minutes after manual tape application to the rostral back.
478 Scorer and experimenter were blinded to genotype.
479
480 For righting reflex measurements, age-matched *S1pr3*$^{-/-}$ and $^{+/+}$ P6-7 neonates were used. Briefly, pups
481 were overturned one at a time on the home cage lid while experimenter was blinded to genotype. The time
482 to righting was measured to the nearest 1/10th of a second with a stopwatch.
483
484 For the CFA model of hypersensitivity, mice were lightly anesthetized with isoflurane (2%) and injected with
485 15 µL CFA (Sigma) into one hindpaw using a Hamilton syringe (30 g) at 5pm. Radiant heat latencies and
486 von Frey 50% withdrawal thresholds were recorded one day prior to CFA, the morning of CFA (prior to
487 injection), and one and two days post-CFA. Von Frey measurements were acquired before radiant heat
488 latencies, and mice were allowed a one-hour recovery period in home cage with access to food and water
489 in between testing. Both ipsilateral and contralateral paw were measured. Experimenter was blind to
490 genotype for injections and recording.
491
492 All behavior experiments were carried out using age-matched or littermate cohorts of male mice and
493 conducted between 8am and 1pm. Mice were tested in 4-part behavior chambers (IITC Life Sciences) with
494 opaque dividers (TAP Plastics) with the exception of righting reflex measurements. Scratching and wiping
495 behaviors were filmed from below using high-definition cameras. All experiments were performed under the
496 policies and recommendations of the International Association for the Study of Pain and approved by the
497 University of California, Berkeley Animal Care and Use Committee.

498

499 *In situ hybridization (ISH)*

500 Fresh DRG were dissected from 8-12 week old mice, flash frozen in OCT embedding medium, and
501 sectioned at 14 µm onto slides. ISH was performed using Affymetrix Quantigene ViewISH Tissue 2-plex kit
502 according to manufacturer's instructions with Type 1 and Type 6 probes. The following probes against
503 mouse mRNAs were created by Affymetrix and used for ISH: *S1pr3, Scn1a, Npy2r, Piezo2, Trpv1, Trpa1.*

504

505 *Immunohistochemistry (IHC) of DRG*

506 DRG were dissected from 8-12 week old adult mice and post-fixed in 4% PFA for one hour. DRG were
507 cryo-protected overnight at 4°C in 30% sucrose-PBS, embedded in OCT, and then sectioned at 12 µm onto
508 slides. Briefly, slides were washed 3x in PBST (0.3% Triton X-100), blocked in 2.5% horse serum + 2.5%
509 BSA PBST, and incubated overnight at 4°C in 1:1000 primary antibody in PBST + 0.5% horse serum +
510 0.5% BSA. Slides were washed 3X in PBS then incubated 1-2 hours at RT in 1:1000 secondary antibody.
511 Slides were washed 3X in PBS and mounted in Fluoromount-G + DAPI with No. 1.5 coverglass. Primary
512 antibodies used: Rabbit anti-DsRed (Clontech #632496), Rabbit anti-S1PR3 (Abcam #38324; #108370),
513 Mouse anti-NF200 (Sigma #N5389), Chicken anti-Peripherin (Abcam #39374). Secondary antibodies used:
514 Goat anti-Mouse Alexa 488 (Abcam #150117), Goat anti-Chicken Alexa 488 (ThermoFisher #A11039),
515 Goat anti-Rabbit Alexa 594 (Invitrogen #R37117). Slides were mounted in Fluoromount with No. 1.5
516 coverglass. Imaging of ISH and DRG IHC experiments, and all live-cell imaging, was performed on an
517 Olympus IX71 microscope with a Lambda LS-xl light source (Sutter Instruments). For ISH and DRG IHC
518 analysis, images were analyzed using ImageJ software. Briefly, DAPI-positive cells were circled and their
519 fluorescence intensity (AFU) for all channels was plotted against cell size using Microsoft Excel software.
520 Co-labeling analysis was performed using ImageJ. Intensity thresholds were set based on the negative
521 control (no probe) slide. Cells were defined as co-expressing if their maximum intensities exceeded the
522 threshold for both channels of interest.

523

524 *IHC of sectioned skin*

525 Skin was dissected from 8 week old adult mice and post-fixed in 4% PFA for 30 minutes at RT. DRG were

526 cryo-protected overnight at 4°C in 30% sucrose-PBS, embedded in OCT, and then sectioned at 18 µm onto
527 slides. Briefly, slides were blocked in 5% normal goat serum in PBST (0.1% Triton X-100) and incubated
528 overnight at 4°C in 1:1000 primary antibody in blocking buffer. Slides were washed 3X in PBS then
529 incubated 45 minutes at RT in 1:1000 secondary antibody. Slides were washed 5X in PBS and mounted in
530 Fluoromount-G + DAPI with No. 1.5 coverglass. Primary antibodies used: Rabbit anti-DsRed (Clontech
531 #632496), Chicken anti-NefH (Abcam #4680), Chicken anti-β-tubulin III (Abcam #107216), mouse anti-
532 PGP9.5 (Abcam #8189). Secondary antibodies used: Goat anti-Mouse Alexa 488 (Abcam #150117), Goat
533 anti-Rabbit Alexa 594 (Invitrogen #R37117), Goat anti-Chicken Alexa 488 (ThermoFisher #A11039). For
534 co-localization analysis, only fibers for which > 50% of the length of the visible fiber contained co-localized
535 (white) pixels were counted. Image analysis was performed using ImageJ.
536
537 *Whole mount skin IHC*
538 Staining was performed according to Marshall and Clary *et al*[71]. Briefly, 8 week old mice were euthanized
539 and the back skin was shaved, depilated, and tape-stripped. The removed skin was fixed overnight in 4%
540 PFA, then washed in PBS (3X for 10 minutes each). Dermal fat was scraped away with a scalpel and skin
541 was washed in PBST (0.3% Triton X-100; 3X for two hours each) then incubated in 1:500 primary antibody
542 (Rabbit anti DsRed: Clontech #632496; Chicken anti-Nefh: Abcam #4680) in blocking buffer (PBST with
543 5% goat serum and 20% DMSO) for 5.5 days at 4°C. Skin was washed as before and incubated in 1:500
544 secondary antibody (Goat anti-Rabbit Alexa 594; Invitrogen #R37117; Goat anti-Chicken Alexa 488;
545 ThermoFisher #A11039) in blocking buffer for 3 days at 4°C. Skin was washed in PBST, serially dried in
546 methanol: PBS solutions, incubated overnight in 100% methanol, and finally cleared with a 1:2 solution of
547 benzyl alcohol: benzyl benzoate (BABB; Sigma) before mounting between No. 1.5 coverglass. Sectioned
548 and whole mount skin samples were imaged on a Zeiss LSM 880 confocal microscope with OPO using a
549 20x water objective. Image analysis was performed using ImageJ.
550
551 *Cell culture*
552 Cell culture was carried out as previously described[72]. Briefly, neurons from dorsal root ganglia (2-8 week
553 old adults) or trigeminal ganglia (P0) were dissected and incubated for 10 min in 1.4 mg ml−1 Collagenase

554 P (Roche) in Hanks calcium-free balanced salt solution, followed by incubation in 0.25% standard trypsin
555 (vol/vol) STV versene-EDTA solution for 2 min with gentle agitation. Cells were then triturated, plated onto
556 Poly D-Lysine coated glass coverslips and used within 20 h. Media: MEM Eagle's with Earle's BSS
557 medium, supplemented with 10% horse serum (vol/vol), MEM vitamins, penicillin/streptomycin and L-
558 glutamine.
559
560 *Calcium imaging*
561 Ca^{2+} imaging experiments were carried out as previously described[72]. Cells were loaded for 60 min at room
562 temperature with 10 μM Fura-2AM supplemented with 0.01% Pluronic F-127 (wt/vol, Life Technologies) in
563 a physiological Ringer's solution containing (in mM) 140 NaCl, 5 KCl, 10 HEPES, 2 CaCl2, 2 MgCl2 and 10
564 D-(+)-glucose, pH 7.4. All chemicals were purchased from Sigma. Acquired images were displayed as the
565 ratio of 340 nm/ 380 nm. Cells were identified as neurons by eliciting depolarization with high potassium
566 Ringer's solution (75 mM) at the end of each experiment. Responding neurons were defined as those
567 having a > 15% increase from baseline ratio. Image analysis and statistics were performed using
568 automated routines in Igor Pro (WaveMetrics). Fura-2 ratios were normalized to the baseline ratio
569 F340/F380 = (Ratio)/(Ratio t = 0).
570
571 *In vitro electrophysiology*
572 Electrophysiological experiments were carried out as previously described[72]. Briefly, recordings were
573 collected at 5 kHz and filtered at 2 kHz (Axopatch 200B, pClamp software). Electrode resistance ranged
574 between 1.5–5 MΩ. Internal solution contained 140 mM KCl, 2 mM MgCl2, 1 mM EGTA, 5 mM HEPES, 1
575 mM Na2ATP, 100 μM GTP, and 100 μM cAMP (pH 7.4). Bath solution was physiological Ringer's solution.
576 The pipette potential was canceled before seal formation. Cell capacitance was canceled before whole cell
577 voltage-clamp recordings. For mechanonociceptors experiments, only cells which were visually identified
578 as mCherry expressing and which had a capacitance between 40-80 pF were used. Rheobase was
579 calculated as the smallest current step required to elicit an action potential using current steps of 50 pA. M

580 currents were measured and analyzed using standard protocols for DRG neurons reported in the
581 literature[30,32,73]. Experiments were carried out only on cells with a series resistance of less than 30
582 MΩ. Analysis of electrophysiology data was performed in pClamp and IgorPro.
583
584 *Ex vivo skin-nerve electrophysiology*
585 Touch-evoked responses in the skin were recorded after dissecting the hind limb skin and saphenous
586 nerve from 7-10 week old mice, according to published methods[74,75]. The skin was placed epidermis-side-
587 up in a custom chamber and perfused with carbogen-buffered synthetic interstitial fluid (SIF) kept at 32 °C
588 with a temperature controller (model TC-344B, Warner Instruments). The nerve was kept in mineral oil in a
589 recording chamber, teased apart, and placed onto a gold recording electrode connected with a reference
590 electrode to a differential amplifier (model 1800, A-M Systems). The extracellular signal was digitized using
591 a PowerLab 8/35 board (AD Instruments) and recorded using LabChart software (AD Instruments).
592
593 For these studies, we focused on A-mechanonociceptors (AMs). To identify responses from these afferents
594 in mutant and control genotypes, we used a mechanical search paradigm with a fine glass probe. Afferents
595 were classified as AMs according to the following criteria: (1) conduction velocity (approximately, 1 to (≤ 12
596 m/s^{-1}), (2) medium-sized receptive fields, (3) sustained response to mechanical indentation[74,76,77].
597
598 Touch-sensitive afferents that did not meet these criteria were not analyzed further. Responses were
599 classified as Adapting AMs if the ratio of mean firing rate in the dynamic phase of stimulation (first 0.2 s) to
600 the static phase of stimulation (last 4.8 s) was greater than 2, and Non-Adapting AMs if the ratio was less
601 than or equal to 2. Non-responders (**Figure 6F**) responded to suprathreshold mechanical stimulation with
602 von Frey monofilaments (tip diameter <0.5 mm), but not to maximal controlled mechanical stimulation (256
603 mN, tip diameter 2 mm). All recordings and analyses were performed blind to genotype.
604
605 Mechanical responses were elicited with von Frey monofilaments and a force controlled custom-built
606 mechanical stimulator. Mechanical thresholds were defined as the lowest von Frey monofilament to reliable

607 elicit at least on action potential. Force controlled mechanical stimuli were delivered using a computer
608 controlled, closed-loop, mechanical stimulator (Model 300C-I, Aurora Scientific, 2 mm tip diameter). Low-
609 pass filtered, 5-second long, length control steps (square wave) simultaneously delivered with permissive
610 force control steps (square wave) were generated using LabChart software (AD Instruments). An arbitrarily
611 selected force step-and-hold protocol (8, 32, 4, 64, 128, 16, 256 mN) was delivered to all fibers. The period
612 between successive displacements was 60 seconds.
613
614 Conduction velocity was measured by electrically stimulating identified receptive fields. Spike sorting by
615 principal component analysis (PCA) and density based clustering, and data analysis was performed off-line
616 with custom-made software in MATLAB. Statistics were performed in Prism.
617
618 *Flow cytometry of CFA-treated hind paws*
619 CFA injections were performed as described above. Briefly, hindpaw skin and underlying fascia of treated
620 and PBS-injected paws were removed from freshly euthanized mice. Skin was placed in RPMI media
621 (Gibco) on ice before mincing with dissection scissors. Digestions were performed for 90 minutes at 37°C
622 on a rotating platform in 1 mL RPMI supplemented with 1:1000 DNaseI enzyme (Roche) and 1 unit
623 LiberaseTM (Roche). Skin was then filtered through 70 µm nylon mesh (Falcon), washed in RPMI, and
624 resuspended in PBS for Aqua Live-Dead staining. Samples were then transferred to FACS buffer (PBS
625 with 0.5% FBS and 2 mM EDTA), blocked, then surface stained with the following antibodies: cKit-Biotin,
626 FceRI-PE, CD49b-PECy7, SiglecF-APC, SA-FITC, Ly6C-PerCP, CD11b-PB, Ly6G-780, CD45.2-AF700
627 (eBiosciences). Compensation tubes (single-stain) were prepared for each fluorophore using positive and
628 negative control beads. A spleen from a wild-type animal was also prepared by crushing between frosted
629 glass slides, straining through 70 µm nylon mesh, and lysing of erythrocytes in ACK (Gibco). A portion of
630 spleen sample was heat-killed for 10 minutes at 65°C and stained with Aqua viability stain and set aside.
631 The rest of the spleen was stained normally with the other skin samples. Samples were then run through a
632 flow cytometer (BD Fortessa). Data were analyzed using FlowJo (Prism) and Microsoft Excel. Neutrophils
633 were defined as live single cells with the following staining profile: $CD45.2^{+}/CD11b^{+}/Ly6G^{+}/Ly6C^{+}$.
634 Inflammatory monocytes were defined as the following: $CD45.2^{+}/CD11b^{+}/Ly6G^{-}/Ly6C^{high}$. Total number of

635 immune cells was reported since neither genotype differed significantly between total number of live cells
636 or total number of CD45.2^{+} immune cells.
637
638 *Statistical analyses*
639 All statistical analyses, except for skin nerve data (see above), were performed using IgorPro software or
640 Microsoft Excel. Values are reported as the mean ± SEM where multiple independent experiments are
641 pooled and reported (for whole cell electrophysiology), and mean ± SD where one experiment was
642 performed with multiple wells (for calcium imaging) or mice (for behavior). For comparison between two
643 groups, Student's unpaired 2-tailed t-test was used. A paired t-test was employed only for measurements
644 within the same biological replicate and after a given treatment. For single-point comparison between >2
645 groups, a one-way ANOVA followed by appropriate post hoc test was used, depending on comparison. For
646 the time course comparison between 2 groups, 2-way ANOVA was used and single comparison p-values
647 were derived using Tukey's HSD or appropriate statistical test, depending on comparison. Number of mice
648 or samples required to attain significance was not calculated beforehand, and where multiple statistical
649 tests were performed, a Bonferroni correction was applied. In figure legends, significance was labeled as:
650 n.s., not significant, $p \geq 0.05$; *$p < 0.05$; **$p < 0.01$; ***$p < 0.001$.
651

652 ## Acknowledgements

653 We thank Z. Rifi (UC Berkeley) for assistance with scoring itch behavior, R. P. Dalton (UC Berkeley) for
654 assistance with confocal microscopy, and P. Lishko and M. Miller (UC Berkeley) for advice on lipid stability
655 and usage. We would also like to thank R. Clary (Columbia) for whole mount skin staining protocols, B.
656 Jenkins (Columbia) for advice on the immunohistochemistry experiments, and D. Julius (UC San

657 Francisco) for the gift of Hm1a spider toxin. Confocal imaging experiments were conducted at the CRL
658 Molecular Imaging Center, supported by the Helen Wills Neuroscience Institute (UC Berkeley). We would
659 like to thank Holly Aaron and Jen-Yi Lee for their microscopy training and assistance. We are grateful to all
660 members of the D.M.B Laboratory (UC Berkeley) for constructive feedback and criticism. The National
661 Institutes of Health grants NS077224 (to D.M.B and R.B.), AR059385 (to D.M.B.), AR051219 (to E.A.L),
662 NS105449 and GM007367 (to B.U.H), and NS063307 (to the Neurobiology Course at the Marine Biological
663 Laboratory); and a Howard Hughes Medical Institute Faculty Scholars grant (to D.M.B) supported this work.
664

665 Competing interests

666 The authors declare no competing interests at this time.

667

668 References

669 1. Caterina, M. J. *et al.* Impaired Nociception and Pain Sensation in Mice Lacking the Capsaicin
670 Receptor. *Science.* **288,** 306–313 (2000).
671 2. Vriens, J. *et al.* TRPM3 Is a Nociceptor Channel Involved in the Detection of Noxious Heat. *Neuron*
672 **70,** 482–494 (2011).
673 3. Ranade, S. S. *et al.* Piezo2 is the major transducer of mechanical forces for touch sensation in mice.
674 *Nature* **516,** 121–125 (2014).
675 4. Woo, S.H. *et al.* Piezo2 is required for Merkel-cell mechanotransduction. *Nature* **509,** 622–626
676 (2014).
677 5. Arcourt, A. *et al.* Touch Receptor-Derived Sensory Information Alleviates Acute Pain Signaling and
678 Fine-Tunes Nociceptive Reflex Coordination. *Neuron* **93,** 179–193 (2017).
679 6. Ghitani, N. *et al.* Specialized Mechanosensory Nociceptors Mediating Rapid Responses to Hair Pull.
680 *Neuron* **95,** 944–954.e4 (2017).
681 7. Duan, B. *et al.* Identification of Spinal Circuits Transmitting and Gating Mechanical Pain. *Cell* **159,**
682 1417–1432 (2014).
683 8. Spiegel, S. & Milstien, S. Sphingosine-1-phosphate: an enigmatic signalling lipid. *Nat Rev Mol Cell*
684 *Biol* **4,** 397–407 (2003).

685 9. Matloubian, M. *et al.* Lymphocyte egress from thymus and peripheral lymphoid organs is dependent
686 on S1P receptor 1. *Nature* **427,** 355–360 (2004).
687 10. Schwab, S. R. *et al.* Lymphocyte sequestration through S1P lyase inhibition and disruption of S1P
688 gradients. *Science* **309,** 1735–1739 (2005).
689 11. Janes, K. *et al.* The development and maintenance of paclitaxel-induced neuropathic pain require
690 activation of the sphingosine 1-phosphate receptor subtype 1. *J. Biol. Chem.* **289,** 21082–21097
691 (2014).
692 12. Mair, N. *et al.* Genetic evidence for involvement of neuronally expressed S1P1 receptor in nociceptor
693 sensitization and inflammatory pain. *PLoS One* **6,** (2011).
694 13. Camprubi-Robles, M. *et al.* Sphingosine-1-phosphate-induced nociceptor excitation and ongoing
695 pain behavior in mice and humans is largely mediated by S1P3 receptor. *J Neurosci* **33,** 2582–2592
696 (2013).
697 14. Brinkmann, V. *et al.* Fingolimod (FTY720): discovery and development of an oral drug to treat
698 multiple sclerosis. *Nat Rev Drug Discov* **9,** 883–897 (2010).
699 15. Couttas, T. a *et al.* Loss of the neuroprotective factor Sphingosine 1-phosphate early in Alzheimer's
700 disease pathogenesis. *Acta Neuropathol. Commun.* **2,** 9 (2014).
701 16. Finley, A. *et al.* Sphingosine 1-phosphate mediates hyperalgesia via a neutrophil-dependent
702 mechanism. *PLoS One* **8,** e55255 (2013).
703 17. Weth, D. *et al.* Activated platelets release sphingosine 1-phosphate and induce hypersensitivity to
704 noxious heat stimuli in vivo. *Front. Neurosci.* **9,** 1–8 (2015).
705 18. Weth-Malsch, D. *et al.* Ablation of Sphingosine 1-Phosphate Receptor Subtype 3 Impairs
706 Hippocampal Neuron Excitability In vitro and Spatial Working Memory In vivo. *Front. Cell. Neurosci.*
707 **10,** 1–12 (2016).
708 19. Usoskin, D. *et al.* Unbiased classification of sensory neuron types by large-scale single-cell RNA
709 sequencing. *Nat. Neurosci.* **18,** 145–153 (2015).
710 20. Zhang, Y. H., Fehrenbacher, J. C., Vasko, M. R. & Nicol, G. D. Sphingosine-1-phosphate via
711 activation of a G-protein-coupled receptor(s) enhances the excitability of rat sensory neurons. *J.*
712 *Neurophysiol.* **96,** 1042–1052 (2006).

713 21. Li, C., Li, J., Kays, J., Guerrero, M. & Nicol, G. D. Sphingosine 1-phosphate enhances the excitability
714 of rat sensory neurons through activation of sphingosine 1-phosphate receptors 1 and/or 3. *J.*
715 *Neuroinflammation* **12,** 1–20 (2015).
716 22. Gerhold, K. *et al.* The Star-Nosed Mole Reveals Clues to the Molecular Basis of Mammalian Touch.
717 *PLoS One* **8,** (2013).
718 23. Kono, M. *et al.* The sphingosine-1-phosphate receptors S1P1, S1P2, and S1P3 function coordinately
719 during embryonic angiogenesis. *J. Biol. Chem.* **279,** 29367–29373 (2004).
720 24. Nussbaum, C. *et al.* Sphingosine-1-phosphate receptor 3 promotes leukocyte rolling by mobilizing
721 endothelial P-selectin. *Nat. Commun.* **6,** 6416 (2015).
722 25. Chiba, Y., Takeuchi, H., Sakai, H. & Misawa, M. SKI-II, an inhibitor of sphingosine kinase,
723 ameliorates antigen-induced bronchial smooth muscle hyperresponsiveness, but not airway
724 inflammation, in mice. *J. Pharmacol. Sci.* **114,** 304–310 (2010).
725 26. Shaner, R. L. *et al.* Quantitative analysis of sphingolipids for lipidomics using triple quadrupole and
726 quadrupole linear ion trap mass spectrometers. *J. Lipid Res.* **50,** 1692–1707 (2009).
727 27. Sanna, M. *et al.* Bitopic S1P3 Antagonist Rescue from Complete Heart Block: Pharmacological and
728 Genetic Evidence for Direct S1P3 Regulation of Mouse Cardiac Conduction. *Mol. Pharmacol.* **89,**
729 176–186 (2015).
730 28. Osteen, J. D. *et al.* Selective spider toxins reveal a role for the Nav1.1 channel in mechanical pain.
731 *Nature* **534,** 494–9 (2016).
732 29. Joost, S. *et al.* Single-Cell Transcriptomics Reveals that Differentiation and Spatial Signatures
733 Shape Epidermal and Hair Follicle Heterogeneity. *Cell Syst.* **3,** 221–237.e9 (2016).
734 30. Schutze, S., Orozco, I. J. & Jentsch, T. J. KCNQ Potassium Channels Modulate Sensitivity of Skin
735 Down hair (D-hair) Mechanoreceptors. *J. Biol. Chem.* **291,** 5566–5575 (2016).
736 31. Passmore, G. M. *et al.* Functional significance of M-type potassium channels in nociceptive
737 cutaneous sensory endings. *Front. Mol. Neurosci.* **5,** 1–12 (2012).
738 32. Crozier, R. A., Ajit, S. K., Kaftan, E. J. & Pausch, M. H. MrgD Activation Inhibits KCNQ / M-Currents
739 and Contributes to Enhanced Neuronal Excitability. *J Neurosci* **27,** 4492–4496 (2007).
740 33. Xu, W. *et al.* Activation of Voltage-Gated KCNQ/Kv7 Channels by Anticonvulsant Retigabine

741 Attenuates Mechanical Allodynia of Inflammatory Temporomandibular Joint in Rats. *Mol. Pain* **6,**
742 1744-8069-6–49 (2010).
743 34. Ramos-Perez, W. D., Fang, V., Escalante-Alcalde, D., Cammer, M. & Schwab, S. R. A map of the
744 distribution of sphingosine 1-phosphate in the spleen. *Nat. Immunol.* **16,** 1245–52 (2015).
745 35. McIlwrath, S. L., Lawson, J. J., Anderson, C. E., Albers, K. M. & Koerber, H. R. Overexpression of
746 neurotrophin-3 enhances the mechanical response properties of slowly adapting type 1 afferents
747 and myelinated nociceptors. *Eur. J. Neurosci.* **26,** 1801–1812 (2007).
748 36. Kwan, K. Y., Glazer, J. M., Corey, D. P., Rice, F. L. & Stucky, C. L. TRPA1 Modulates
749 Mechanotransduction in Cutaneous Sensory Neurons. *J. Neurosci.* **29,** 4808–4819 (2009).
750 37. Smith, A. K., O'Hara, C. L. & Stucky, C. L. Mechanical sensitization of cutaneous sensory fibers in
751 the spared nerve injury mouse model. *Mol. Pain* **9,** 1–6 (2013).
752 38. Garrison, S. R., Dietrich, A. & Stucky, C. L. TRPC1 contributes to light-touch sensation and
753 mechanical responses in low-threshold cutaneous sensory neurons. *J. Neurophysiol.* **107,** 913–922
754 (2012).
755 39. Ghasemlou, N., Chiu, I. M., Julien, J.-P. & Woolf, C. J. CD11b $^{+}$ Ly6G $^{-}$ myeloid cells mediate
756 mechanical inflammatory pain hypersensitivity. *Proc. Natl. Acad. Sci.* 201501372 (2015).
757 doi:10.1073/pnas.1501372112
758 40. Abrahamsen, B. *et al.* The Cell and Molecular Basis of Mechanical, Cold, and Inflamatory Pain.
759 *Science.* **321,** 702 (2008).
760 41. Lennertz, R. C., Kossyreva, E. A., Smith, A. K. & Stucky, C. L. TRPA1 mediates mechanical
761 sensitization in nociceptors during inflammation. *PLoS One* **7,** 1–11 (2012).
762 42. Chalfant, C. E. & Spiegel, S. Sphingosine 1-phosphate and ceramide 1-phosphate: expanding roles
763 in cell signaling. *J. Cell Sci.* **118,** 4605–4612 (2005).
764 43. Pappu, R. *et al.* Promotion of lymphocyte egress into blood and lymph by distinct sources of
765 sphingosine-1-phosphate. *Science* **316,** 295–298 (2007).
766 44. Morita, T. *et al.* HTR7 Mediates Serotonergic Acute and Chronic Itch. *Neuron* **87,** 124–138 (2015).
767 45. Szczot, M. *et al.* Cell-Type-Specific Splicing of Piezo2 Regulates Mechanotransduction. *Cell Rep.*
768 **21,** 2760–2771 (2017).

769 46. Passmore, G. M. *et al.* KCNQ/M currents in sensory neurons: significance for pain therapy. *J.*
770 *Neurosci.* **23,** 7227–7236 (2003).
771 47. Hayashi, H., Iwata, M., Tsuchimori, N. & Matsumoto, T. Activation of peripheral KCNQ channels
772 attenuates inflammatory pain. *Mol. Pain* **10,** 15 (2014).
773 48. Blackburn-Munro, G. & Jensen, B. S. The anticonvulsant retigabine attenuates nociceptive
774 behaviours in rat models of persistent and neuropathic pain. *Eur. J. Pharmacol.* **460,** 109–116
775 (2003).
776 49. Ray, P. *et al.* Comparative transcriptome profiling of the human and mouse dorsal root ganglia: An
777 RNA-seq-based resource for pain and sensory neuroscience research. *bioRxiv* 165431 (2017).
778 doi:10.1101/165431
779 50. Flegel, C. *et al.* RNA-Seq analysis of human trigeminal and dorsal root ganglia with a focus on
780 chemoreceptors. *PLoS One* **10,** 1–30 (2015).
781 51. Young, G. T. *et al.* Characterizing human stem cell-derived sensory neurons at the single-cell level
782 reveals their ion channel expression and utility in pain research. *Mol. Ther.* **22,** 1530–1543 (2014).
783 52. Oetjen, L. K. *et al.* Sensory Neurons Co-opt Classical Immune Signaling Pathways to Mediate
784 Chronic Itch. *Cell* **129,** 742–751 (2017).
785 53. Pinho-Ribeiro, F. A., Verri, W. A. & Chiu, I. M. Nociceptor Sensory Neuron–Immune Interactions in
786 Pain and Inflammation. *Trends Immunol.* **38,** 5–19 (2017).
787 54. Donoviel, M. S. *et al.* Spinster 2, a sphingosine 1-phosphate transporter, plays a Critical Role in
788 inflammatory and Autoimmune Diseases. *FASEB J.* **29,** 5018–5028 (2015).
789 55. Gräler, M. H. & Goetzl, E. J. The immunosuppressant FTY720 down-regulates sphingosine 1-
790 phosphate G-protein-coupled receptors. *FASEB J.* **18,** 551–553 (2004).
791 56. Olivera, A., Allende, M. L. & Proia, R. L. Shaping the landscape: Metabolic regulation of S1P
792 gradients. *Biochim. Biophys. Acta - Mol. Cell Biol. Lipids* **1831,** 193–202 (2013).
793 57. Allende, M. L. *et al.* Sphingosine-1-phosphate lyase deficiency produces a pro-inflammatory
794 response while impairing neutrophil trafficking. *J. Biol. Chem.* **286,** 7348–7358 (2011).
795 58. Kunkel, G. T., Maceyka, M., Milstien, S. & Spiegel, S. Targeting the sphingosine-1-phosphate axis in
796 cancer, inflammation and beyond. *Nat. Rev. Drug Discov.* **12,** 688–702 (2013).

797 59. Roviezzo, F. *et al.* S1P-induced airway smooth muscle hyperresponsiveness and lung inflammation
798 in vivo: Molecular and cellular mechanisms. *Br. J. Pharmacol.* **172,** 1882–1893 (2015).
799 60. Liang, J. *et al.* Sphingosine-1-Phosphate Links Persistent STAT3 Activation, Chronic Intestinal
800 Inflammation, and Development of Colitis-Associated Cancer. *Cancer Cell* **23,** 107–120 (2013).
801 61. Rivera, J., Proia, R. L. & Olivera, A. The alliance of sphingosine-1-phosphate and its receptors in
802 immunity. *Nat. Rev. Immunol.* **8,** 753–763 (2008).
803 62. Myśliwiec, H. *et al.* Increase in circulating sphingosine-1-phosphate and decrease in ceramide levels
804 in psoriatic patients. *Arch. Dermatol. Res.* (2016). doi:10.1007/s00403-016-1709-9
805 63. Checa, A. *et al.* Circulating levels of sphingosine-1-phosphate are elevated in severe, but not mild
806 psoriasis and are unresponsive to anti-TNF-α treatment. *Sci. Rep.* **5,** 12017 (2015).
807 64. Grenald, S. A. *et al.* Targeting the S1P/S1PR1 axis mitigates cancer-induced bone pain and
808 neuroinflammation. *Pain* **158,** 1 (2017).
809 65. Trankner, D., Hahne, N., Sugino, K., Hoon, M. A. & Zuker, C. Population of sensory neurons
810 essential for asthmatic hyperreactivity of inflamed airways. *Proc. Natl. Acad. Sci.* **111,** 11515–11520
811 (2014).
812 66. Wilson, S. R. *et al.* The Ion Channel TRPA1 Is Required for Chronic Itch. *J. Neurosci.* **33,** 9283–
813 9294 (2013).
814 67. Tsunozaki, M. *et al.* A 'toothache tree' alkylamide inhibits Aδ mechanonociceptors to alleviate
815 mechanical pain. *J. Physiol.* **591,** 3325–40 (2013).
816 68. Shimada, S. G. & LaMotte, R. H. Behavioral differentiation between itch and pain in mouse. *Pain*
817 **139,** 681–687 (2008).
818 69. Chaplan, S.R., Bach, F.W., Pogrel, J.W., Chung, J.M., Yaksh, T. Quantitative assessment of tactile
819 allodynia evoked by unilateral ligation of the fifth and sixth lumbar nerves in the rat. *J. Neurosci.* **53,**
820 55–63 (1994).
821 70. Dixon, W. J. The Up-and-Down Method for Small Samples. *J. Am. Stat. Assoc.* **60,** 967–978 (1980).
822 71. Marshall, K. L. *et al.* Touch Receptors Undergo Rapid Remodeling in Healthy Skin. *Cell Rep.* **17,**
823 1719–1727 (2016).
824 72. Wilson, S. R. *et al.* TRPA1 is required for histamine-independent, Mas-related G protein-coupled

825 receptor-mediated itch. *Nat. Neurosci.* **14,** 595–602 (2011).

826 73. Zheng, Q. *et al.* Suppression of KCNQ/M (Kv7) potassium channels in dorsal root ganglion neurons
827 contributes to the development of bone cancer pain in a rat model. *Pain* **154,** 434–448 (2013).

828 74. Wellnitz, S. A., Lesniak, D. R., Gerling, G. J. & Lumpkin, E. A. The Regularity of Sustained Firing
829 Reveals Two Populations of Slowly Adapting Touch Receptors in Mouse Hairy Skin. *J.*
830 *Neurophysiol.* **103,** 3378–3388 (2010).

831 75. Maksimovic, S. *et al.* Epidermal Merkel cells are mechanosensory cells that tune mammalian touch
832 receptors. *Nature* **509,** 617–621 (2014).

833 76. Koltzenburg, M. *et al.* Receptive Properties of Mouse Sensory Neurons Innervating Hairy Skin
834 Receptive Properties of Mouse Sensory Neurons Innervating Hairy Skin. *J. Neurophysiol.* **78,** 1841–
835 1850 (1997).

836 77. Zimmermann, K. *et al.* Phenotyping sensory nerve endings in vitro in the mouse. *Nat. Protoc.* **4,**
837 174–196 (2009).

838

839

840 ## Figure captions

841 **Figure 1. S1PR3 mediates acute mechanical pain. A.** von Frey 50% withdrawal threshold
842 measurements for *S1pr3*$^{+/+}$ (WT, N = 8), $^{+/-}$ (HET, N = 7) and $^{-/-}$ (KO, N = 12) mice. $p < 0.0001$ (one-way
843 ANOVA). Tukey-Kramer post hoc comparisons for KO and HET to WT indicated on graph. **B.** von Frey
844 force-response graph for WT (N = 8) versus KO (N = 12) animals; $p_{genotype} < 0.0001$ (two-way ANOVA).
845 Tukey HSD comparisons between genotypes are indicated for given forces. **C.** % withdrawal to pinprick
846 stimulation of hindpaw for HET versus KO animals; $p < 0.0001$ (unpaired t-test; N = 5-7 mice per group). **D.**
847 Number of attempted removal bouts in tape assay for WT (N =2), HET (N = 2), and KO (N = 5) mice; $p =$
848 0.172 (one-way ANOVA). **E.** Baseline radiant heat measurements for WT, HET, and KO mice. N = 8 WT, 3
849 HET, and 5 KO mice. $p = 0.444$ (one-way ANOVA). **F.** von Frey 50% withdrawal threshold measurements
850 for mice pre- and post-injection of 500 μM TY 52156 (N = 10), 10 μM W146 (N = 6), or 1% DMSO-PBS
851 vehicle (N = 17); $p = 0.016$, 0.650 (two-tailed paired t-test comparing vehicle- vs. drug-injected paw). **G.**
852 von Frey force-response graph for mice injected with either 1% DMSO-PBS or 500 μM TY 52156; $p_{treatment}$ <

853 1e-05 (two-way ANOVA; N = 4 mice per group). Tukey HSD comparisons were made between treatment
854 groups and significant differences at a given force are indicated on graph. Error bars represent mean ± SD.
855
856 **Figure 1-source data 1. S1PR3 mediates acute mechanical pain.** *Related to Figure 1.*
857
858 **Figure 1-figure supplement 1. Loss of S1PR3 selectively impairs mechanonociception.** *Related to*
859 *Figure 1.* **A.** Time to righting in seconds for N = 6 P7 pups per genotype for WT and KO mice; p = 0.575
860 (two-tailed unpaired t-test). **B.** (Left) Time spent scratching in response to injection of 50 mM chloroquine or
861 PBS vehicle (VEH) in WT and KO mice; p = 0.36, 0.98, (unpaired t-tests; N = 3-4 mice per group). (Right)
862 Time spent scratching in response to injection of 27 mM Histamine or 0.1% DMSO-PBS in WT and KO
863 mice; p = 0.51, 0.06 (unpaired t-tests; N = 3-4 mice per group). **C.** Normalized paw withdrawal latencies
864 post-injection of SKI II, TY 52156, or 0.1% DMSO-PBS vehicle into the hind paw of wild-type animals; p =
865 0.65 (one-way ANOVA); N = 5 mice per group. Unless otherwise indicated, error bars represent mean ±
866 SD.
867
868 **Figure 2. Endogenous S1P mediates acute mechanical pain. A.** von Frey 50% withdrawal
869 measurements for mice pre- and post-injection of 50 μM SKI II (N = 8) or 10 μM S1P (N = 7); p = 0.003,
870 0.604 (two-tailed paired t-tests). **B.** von Frey force-response graph for animals injected with 10 μM S1P or
871 0.1% MeOH-PBS; $p_{genotype}$ > 0.05 (two-way ANOVA; N = 8 mice per group). No Tukey HSD comparisons
872 at any force between genotypes were significant. **C.** Intradermal cheek injection of 10 μM S1P, 2 μM, 0.2
873 μM, and 20 μL 0.3% methanol PBS (vehicle), with quantification of number of forepaw wipes over the 5
874 minute post-injection interval; p < 0.0001 (one-way ANOVA; N = 3 mice per condition). Dunnett's multiple
875 comparisons p-values are represented on graph for comparisons made between treated and vehicle
876 groups. **D.** Radiant heat normalized paw withdrawal latencies 20-30 minutes post injection of 15 μL 10 μM
877 S1P, 0.2 μM S1P. or 0.3% methanol-PBS vehicle (i.d.) into the hind paw of S1PR3 WT or KO mice; p =
878 0.0129 (one-way ANOVA; N = 3-10 mice per condition). Dunnett's multiple comparisons p-values are
879 represented on graph for comparisons made between treated and vehicle groups. **E.** von Frey 50%
880 withdrawal measurements for mice pre- (baseline) and post-injection of 50 μM SKI II (N = 14) and 0, 10,

881 75, or 200 nM S1P (one-way ANOVA, p = 0.0001; N = 4, 3, 4, 3 animals). Tukey Kramer comparisons are
882 indicated on graph. Error bars represent mean ± SD.
883
884 **Figure 2-source data 2. Endogenous S1P mediates acute mechanical pain.** *Related to Figure 2.*
885
886 **Figure 3. *S1pr3* is expressed in A mechanonociceptors and C thermal nociceptors. A.** (Top)
887 Representative co-ISH of *S1pr3* (green; left) with *Scn1a*, *Npy2r*, *Piezo2*, and *Trpv1* (magenta; center) in
888 sectioned DRG. Right column: overlay with co-localized regions colored white (10x air objective; scale =
889 100 µm). **B.** Bar chart showing the % of total cells expressing the indicated marker (grey) and the % of total
890 cells co-expressing both marker and *S1pr3* (green). See Table S1 for quantification. **C.** Representative IHC
891 images of sectioned DRG from *S1pr3*$^{mCherry/+}$ animals stained with anti-DsRed (green, S1PR3) and anti-
892 Peripherin (left, magenta) or anti-NF200 (right, magenta). Arrows indicate co-stained cells. Images were
893 acquired using a 10x air objective (scale = 100 µm). **D.** Whole-mount skin IHC confocal images with anti-
894 DsRed antibody (S1PR3, green) and anti-NefH antibody (NF200, magenta) in an *S1pr3*$^{mCherry/+}$ animal (20x
895 water objective; scale = 50 µm). Arrows indicate co-positive free nerves (left image). Arrowheads indicate
896 NF200- free nerves (left) or S1PR3- circumferential fibers (right image). **E.** Sectioned skin IHC with anti-
897 DsRed (S1PR3) and anti-NefH (NF200, left, top right) or anti-DsRed (S1PR3) and anti-beta-tubulin III
898 (BTIII, bottom right) antibody (magenta) in *S1pr3*$^{mCherry/+}$ skin (20x air objective; scale = 50 µm). Arrows
899 indicate co-positive free nerve endings (left), S1PR3-negative lanceolate/circumferential hair follicle
900 endings (top right, arrow = circumferential, arrowhead = lanceolate), or S1PR3-negative putative Merkel
901 afferent (bottom right). **F.** (Left) Quantification of sectioned DRG IHC experiments showing % of S1PR3+
902 cells that co-stained with indicated markers (n > 250 cells per marker). (Right) Quantification of sectioned
903 skin IHC experiments showing % of fibers positive for indicated marker that co-stained with S1PR3 (anti-
904 DsRed; n = 10 images per marker from 2 animals).
905
906 **Figure 3-figure supplement 1. S1PR3 KO animals display normal representation of somatosensory**
907 **neuronal subtypes.** *Related to Figure 3.* **A.** ISH of sectioned adult DRG from WT and S1PR3 KO animals
908 showing specificity of *S1pr3* probes (20x air objective, scale = 50 µm). **B.** (Image) Representative ISH

909 *Trpv1* (top) and *Trpa1* (bottom) from sectioned DRG of wild-type (left) and S1PR3 KO animals (right; 20x
910 air objective; scale = 50 μm). **C.** % of total cells expressing *Trpv1* and *Trpa1* in sectioned DRG of wild-type
911 and S1PR3 KO animals. **D.** (Left) Average diameter ± SEM of all cells in sectioned DRG from WT and
912 S1PR3 KO animals (p = 0.36, t-test; n = 437 and 679 cells from two animals each, respectively). (Right)
913 Average diameter ± SD of *Trpv1+* cells in WT and S1PR3 KO DRG (p = 0.63, t-test; n = 127 and 85 cells
914 respectively). **E.** Representative staining with anti-S1PR3 antibody (1:2000) in sectioned adult DRG from
915 WT and S1PR3 KO animals (10x air objective, scale = 100 μm). **F.** Representative IHC images of
916 sectioned DRG from S1PR3 KO animals stained with anti-DsRed (green) and anti-Peripherin (left,
917 magenta) or anti-NF200 (right, magenta). Images were acquired using a 10x air objective (scale = 100 μm).
918 **G.** (Left) Quantification of total percentage of cells stained with indicated markers in sectioned DRG from
919 *S1pr3*$^{mCherry/+}$ and S1PR3 KO animals (n > 250 cells per condition). (Right) Average diameter of anti-
920 NF200+ cells in *S1pr3*$^{mCherry/+}$ and S1PR3 KO DRG (p = 0.15, t-test; n = 256 and 194 cells, respectively). **H.**
921 Percent responders to S1P and capsaicin in ratiometric calcium imaging of wild-type and *S1pr3* $^{-/-}$ cultured
922 DRG and TG neurons; p < 0.0001 (one-way ANOVA; N = 2 DRG and 2 TG preparations of 8 wells each).
923 Sidak's multiple comparisons p-values are represented on graph for comparisons made between
924 genotypes. Error bars represent mean ± SEM. **I.** (Left) No primary control showing robust staining of hair
925 follicles in whole mount skin in contrast to specific neuronal staining shown in **Figure 3D**. (Right) No
926 primary control showing staining around hair follicles and in epidermis in sectioned skin. Scale = 50 μm
927 (20x water objective).
928
929 **Supplementary file 1. Co-ISH quantification for sectioned DRG from adult wild-type mice.** *Related to*
930 *Figure 3.*
931
932 **Figure 4. S1P activates thermal nociceptors but not mechanonociceptors. A.** (Left) Representative
933 image of mCherry signal in live, cultured adult DRG neurons from one *S1pr3*$^{mCherry/+}$ animal. (Right)
934 Quantification of % of total cells expressing *S1pr3* from DRG ISH and mCherry from dissociated DRG
935 cultures (N = 2 animals each experiment). **B.** Representative traces depicting F340/F380 signal from
936 Fura2-AM calcium imaging showing two neurons, one which responded to 1 μM S1P, 1 μM Capsaicin, and

937 high K+ Ringer's (red) and one which only responded to high K+ (black). **C.** (Left) Fura-2 AM calcium
938 imaging before (left) and after (center) addition of 1 μM S1P in *S1pr3* $^{mCherry/+}$ cultured mouse DRG neurons.
939 Bar indicates fluorescence ratio. Right-hand image indicates mCherry fluorescence. (Right) % of mCherry
940 neurons that are responsive to 1 μM S1P in ratiometric calcium imaging (n > 1000 cells from 16 imaging
941 wells from three animals). **D.** Dose-response curve of mean neuronal calcium responders to varying
942 concentrations of S1P. Concentrations used: 1, 10, 50, 100, 200, 1000, and 10,000 nanomolar. Error bars
943 represent mean ± SD (N = 2 animals). Black dotted line indicates sigmoidal fit for all S1P responders from
944 which EC_{50} was derived. All S1P responders were also capsaicin-responsive. **E.** Current-clamp trace of a
945 single wild-type neuron firing action potentials in response to bath addition of 1 μM S1P and 1 μM
946 capsaicin, with Ringer's wash in-between. n = 4 of 10 neurons responded to S1P and N = 1 of 1 S1P-
947 responsive also responded to capsaicin. Bar = 2 seconds. **F.** (Left) Fura-2 AM calcium imaging after
948 addition of 500 nM Hm1a in *S1pr3*$^{mCherry/+}$ P0 TG neurons, which were instead of adult DRG neurons
949 because they respond to Hm1a without prior PGE_2 sensitization. Right-hand image indicates mCherry
950 fluorescence. (Right) % of Hm1a-responsive P0 TG neurons that are mCherry+ (N = 1 animal, 1230 total
951 neurons).
952
953 **Figure 5. S1PR3 modulates KCNQ2/3 channels to regulate AM excitability.** All experiments were
954 performed in *S1pr3*$^{mCherry/+}$ or $^{-/-}$ DRG neurons. **A.** (Left) Example traces of a single mCherry+ neuron in
955 whole cell current clamp before and after S1P application. (Right) % change in rheobase after S1P
956 application for *S1pr3*$^{mCherry/+}$ (left) and KO (right) neurons ($p_{WT,KO}$ = 0.012, 0.287; two-tailed paired t-tests; N
957 = 7, 12 cells). **B.** % Δ in input resistance after S1P or vehicle application (p = 0.017; two-tailed paired t-
958 test; N = 4 cells per group). **C.** Instantaneous current-voltage relationship after subtraction of the post-S1P
959 current from the pre-S1P current. Current reverses at -60.125 mV; N = 6 cells. Data were fitted with a
960 Boltzmann equation. A pre-pulse stimulation of +100 mV for 100 ms was used. Unless indicated otherwise,
961 all error bars represent mean ± SEOM. **D.** % Δ in inward tail current after S1P or 1% DMSO vehicle
962 application for *S1pr3*$^{mCherry/+}$ and KO medium-diameter neurons using a step to +80 mV followed by a step
963 to -80 mV (p = 0.014; one-way ANOVA; N = 10, 13, 10 cells). Tukey Kramer post hoc p-values indicated
964 on graph. **E.** (Graphic, top) Averaged current traces of a single mCherry+ neuron in whole cell voltage

965 clamp recording pre- and post-S1P using indicated voltage step protocol. (graphic, bottom) Averaged
966 current traces of a single mCherry+ neuron in whole cell voltage clamp recording with XE991 treatment.
967 Holding phase (-40 mV, 150 ms) was truncated in traces. (Left graph) % Δ in outward tail current (average
968 +/- SD after indicated treatments (1 μM S1P, 3 μM XE 991, or both) for *S1pr3*$^{mCherry/+}$ medium-diameter
969 neurons; (p = 0.58; one-way ANOVA; n = 6, 8, 14 cells) using protocol depicted at right. (Right graph) % Δ
970 in inward tail current after indicated treatments (LINO = 100 μM linopirdine) for *S1pr3*$^{mCherry/+}$ medium-
971 diameter neurons; (p = 0.47; two-tailed paired t-test; N = 12 cells).
972
973 **Figure 5-source data 1. S1PR3 modulates KCNQ2/3 channels to regulate AM excitability.** *Related to*
974 *Figure 5.*
975
976 **Figure 5-figure supplement 1. S1P selectively modulates potassium tail currents to increase DRG**
977 **neuron excitability.** *Related to Figure 5.* **A.** (Left) Example trace of a single mCherry+ neuron in S1P
978 before and after current injection. (Right) Resting membrane potential (RMP) in millivolts before and after
979 addition of S1P (p = 0.23; two-tailed paired t-test; n = 6 cells). **B.** Rheobase pre- and post-S1P application
980 in DRG neurons; p_{WT} = 0.011; p_{KO} = 0.28 (two-tailed paired t-test). Same data are represented in Figure
981 5A. **C.** Sodium I-V relationship for a representative *S1pr3*$^{mCherry/+}$ medium-diameter neuron pre- and 5
982 minutes post- 1 μM S1P using voltage step from -100 to +80 mV (150 ms steps, -80 mV holding). **D.**
983 Steady-state I-V relationship for same neuron. **E.** (Left) % Δ in peak instantaneous sodium current after
984 S1P or 1% DMSO vehicle application for medium-diameter mCherry+ neurons; p = 0.39 (two-tailed paired
985 t-test; n = 7 cells per group). (Right) % Δ in peak steady-state current after S1P or 1% DMSO vehicle
986 application for medium-diameter mCherry+ neurons; p = 0.948 (two-tailed paired t-test; n = 7 cells per
987 group). **F.** Dose-response relationship between % Δ in tail current and S1P concentration for 1 nM, 50 nM,
988 100 nM, and 1 μM S1P (n = 7 cells). EC_{50} (48.8 nM), marked by thin dotted lines, was estimated from
989 sigmoidal fit (thick dotted line).
990
991 **Figure 6. S1PR3 is required for nociceptive responses of high-threshold AM nociceptors. A.** (Left)
992 Representative traces of AM fiber activity over time in *ex vivo* skin-saphenous nerve recording in response

993 to stimulation (128 mN, top) from HET (middle) and KO (bottom) mice. (Right) Mean firing rate of AM fibers
994 in response to force controlled stimulation (4,8,16,32,64,128,256 mN). ***p*=0.001, ****p*=0.0002 (two-way
995 ANOVA, Sidak's post-hoc); lines, linear regression (HET: slope, 50 Hz/N, R^2, 0.99; KO: slope, 35 Hz/N, R^2,
996 0.95). **B.** von Frey threshold of AM fibers in S1PR3 HET and KO skin. ****p* < 0.0001 (Mann-Whitney test);
997 lines, median; boxes, 25-75 percentile; whiskers, min-max. **C.** Conduction velocity (CV) of AM fibers in
998 S1PR3 HET and KO mice. *p* = 0.65 (two-tailed t-test); n = 40, 36 fibers; errors, mean ± SEM. **D.**
999 Cumulative response plot of AM fibers to force controlled stimulation (solid lines); four-parameter logistic fit
1000 from which half-maximal force was estimated for each genotype (dotted lines). **E.** Representative traces of
1001 Non-Adapting and Adapting AMs in response to force controlled stimulation (256 mN, top) for S1PR3 HET
1002 and KO mice; blue regions, dynamic phase of stimulation. **F**. Proportion of fibers classified by pattern of
1003 mechanically evoked responses to 256 mN of stimulation: Non-Responder (HET, 2/40 fibers; KO 5/36),
1004 Non-Adapting AM (HET, 18/40; KO, 29/36), Adapting AM (HET, 20/40; KO, 2/36). Non-Responders fired
1005 action potentials to large magnitude von Frey monofilaments (<0.5 mm tip diameter), but not to 256 mN of
1006 controlled mechanical stimulation (2 mm tip diameter). Classification of Non-Adapting vs. Adapting AMs
1007 detailed in methods. ****p*<0.00001 (Chi-square test).
1008
1009 **Figure 6-source data 1. S1PR3 is required for nociceptive responses of high-threshold AM**
1010 **nociceptors.** *Related to Figure 6.* Table provides properties of all S1PR3 HET and KO AM fibers that were
1011 recorded.
1012
1013 **Figure 6-figure supplement 1. S1PR3 +/- AM nociceptors display normal nociceptive responses.**
1014 *Related to Figure 6*. **A.** Mean firing rate of AM fibers in response to force controlled stimulation
1015 (4,8,16,32,64,128,256 mN) from **Figure 6A**, with additional data from one wild-type animal (n_{WT} = 4 fibers)
1016 (WT: slope, 57 Hz/N, R^2, 0.98; *p* = 0.90, two-way ANOVA comparing HET and WT). **B.** (Left) Collected
1017 conduction velocities from teased fibers from 6 S1PR3 KO animals (purple, Ab, centroid=13.1 m/s; yellow,
1018 Ad, centroid=5.7 m/s; orange, C, centroid=0.4 m/s; R^2 =0.69, N = 65 fibers). (Right) Collected conduction
1019 velocities from teased fibers from 1 S1PR3 HET and 6 WT animals (purple, Ab, centroid=14.5 m/s; yellow,

1020 Ad, centroid=6.8 m/s; orange, C, centroid=0.3 m/s; R^2 =0.82, N = 76 fibers). Three-term Gaussian model.
1021 X-axis plotted on a log 1.2 scale.
1022
1023 **Figure 7. S1PR3 is dispensable for development of chronic mechanical hypersensitivity. A.** Thermal
1024 latency before and after CFA treatment (indicated by dotted line); $p_{genotype}$ = 0.0053 (two-way ANOVA; N = 5
1025 mice per genotype). Sidak's multiple comparison between genotypes for specific time points indicated on
1026 graph. Error bars represent mean ± SD. **B.** (Left) Normalized 50% withdrawal threshold before and after
1027 CFA treatment (indicated by dotted line); *p*(genotype) < 0.001 (two-way ANOVA). (Right) 50% withdrawal
1028 thresholds for same experiment (*p(*genotype) = 0.1634; two-way ANOVA). **C.** (Left) Thermal latency
1029 assessed before ("Baseline") and 24 hours post CFA injection with either vehicle (CFA + VEH) or TY 52156
1030 (CFA + TY) acutely administered; *p* < 0.0001 (one-way ANOVA N = 5 mice per treatment). (Right) Thermal
1031 latency assessed before and after CFA injection with either vehicle (VEH) or SKI II acutely administered on
1032 Day 1; *p* < 0.0001 (one-way ANOVA; N = 5-7 mice per treatment). Dunnett's test comparisons to baseline
1033 are indicated on graph. Error bars represent mean ± SD. **D.** (Left) 50% withdrawal threshold assessed
1034 before and 24 hours post CFA injection with either vehicle (CFA + VEH) or TY 52156 (CFA + TY) acutely
1035 administered on Day 1; *p* < 0.0001 (one-way ANOVA; N = 5 mice per treatment). Dunnett's test
1036 comparisons to baseline are indicated on graph. (Right) 50% withdrawal threshold assessed before and
1037 24 hours post CFA injection with either vehicle (CFA + VEH) or SKI II (CFA + SKI II) acutely administered;
1038 *p*-values indicated on graph (two-tailed unpaired t-test; N = 5 mice per group.
1039
1040 **Figure 7-source data 1. S1PR3 is dispensable for development of chronic mechanical**
1041 **hypersensitivity.** *Related to Figure 7.*
1042
1043 **Figure 7-figure supplement 1. S1PR3 KO animals display normal CFA-evoked immune cell**
1044 **recruitment.** *Related to Figure 7.* **A.** Recruitment of neutrophils (Neut.) or inflammatory monocytes (IMs)
1045 to hindpaw skin 24 hours post-CFA administration in S1PR3 HET and KO mice, as a dot plot of CD11b+
1046 cells plotting Ly6G fluorescence intensity vs. Ly6C intensity (AFU). Boxes are for illustrative purposes. **B.**
1047 Recruitment of immune cells, including neutrophils (Neut.) and inflammatory monocytes (IMs) to hindpaw

1048 skin 24 hours post-CFA administration in HET and KO mice, displayed as total number of cells; N = 8 mice
1049 per genotype. Sidak's multiple comparisons were made between HET and KO for each cell type.
1050
1051 **Figure 8. Proposed model illustrating a key role for S1PR3 in regulating mechanical pain in AM**
1052 **nociceptors.** (Top) S1P promotes activation of S1PR3, which leads to inhibition of KCNQ2/3 currents and
1053 promotes normal mechanical pain sensitivity. (Bottom) Diminished S1P or S1PR3 antagonism alleviates
1054 inhibition of KCNQ2/3, leading to mechanical pain hyposensitivity.

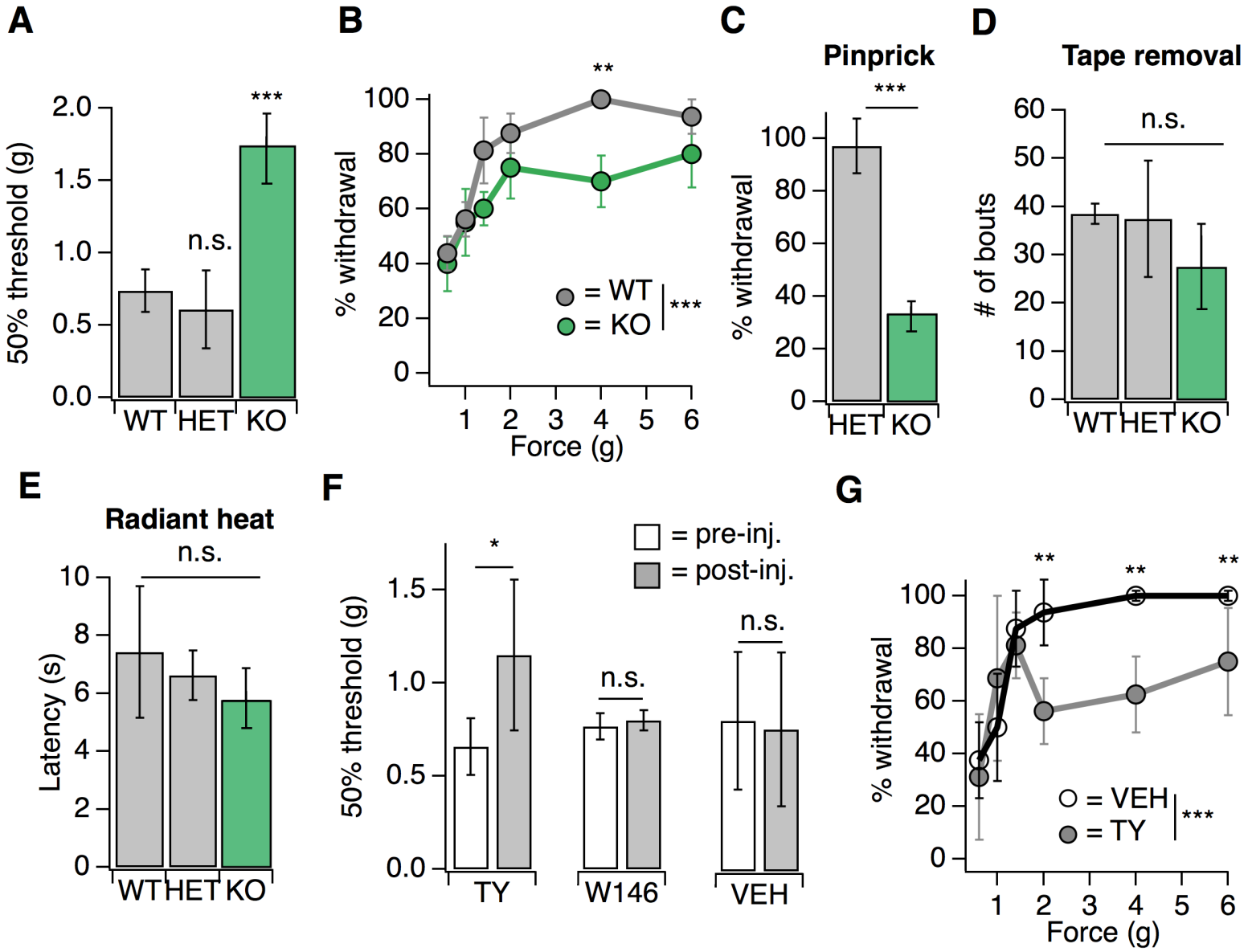
A
50% threshold (g)
2.0
1.5
1.0
0.5
0.0
***
n.s.
WT
HET
KO
B
% withdrawal
100
80
60
40
20
0
**
= WT
= KO
***
1
2
3
4
5
6
Force (g)
C
Pinprick
% withdrawal
100
80
60
40
20
0
***
HET
KO
D
Tape removal
# of bouts
60
50
40
30
20
10
0
n.s.
WT
HET
KO
E
Radiant heat
Latency (s)
10
8
6
4
2
0
n.s.
WT
HET
KO
F
50% threshold (g)
1.5
1.0
0.5
0.0
= pre-inj.
= post-inj.
*
n.s.
n.s.
TY
W146
VEH
G
% withdrawal
100
80
60
40
20
0
**
**
**
= VEH
= TY
***
1
2
3
4
5
6
Force (g)

Figure 1

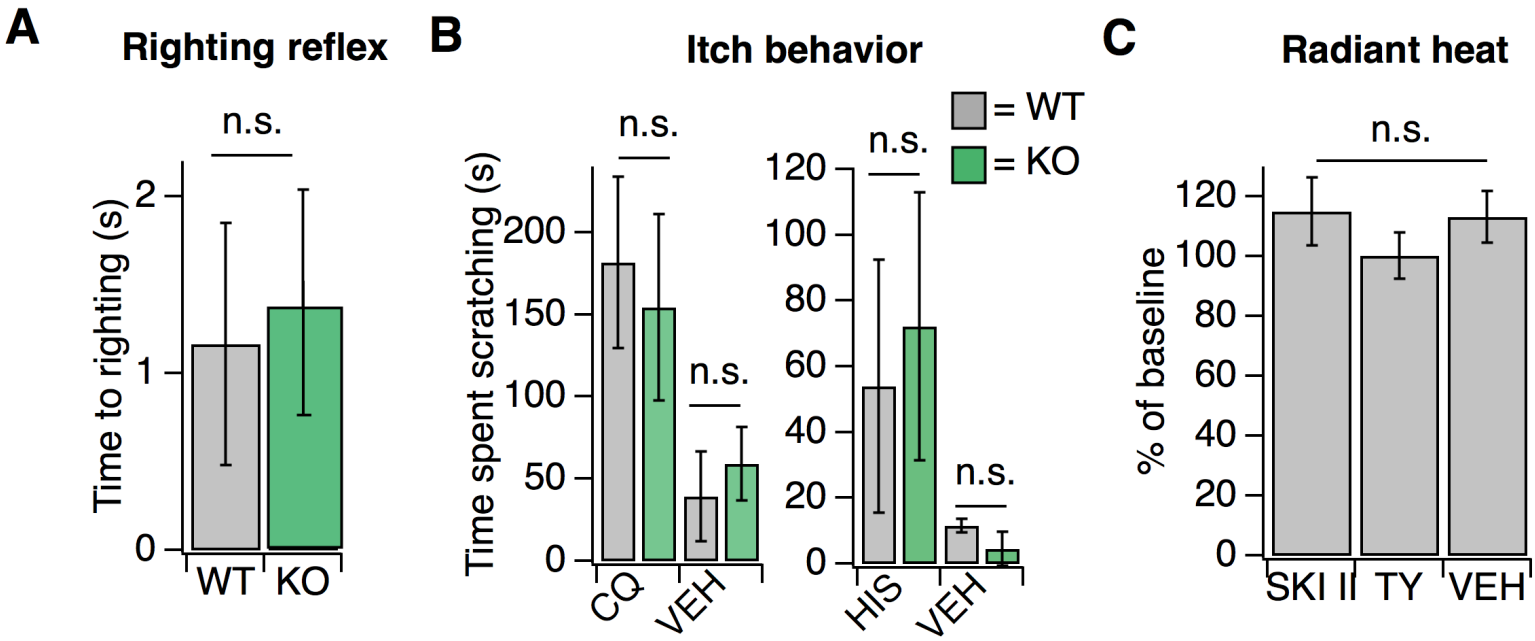

Figure 1-figure supplement 1

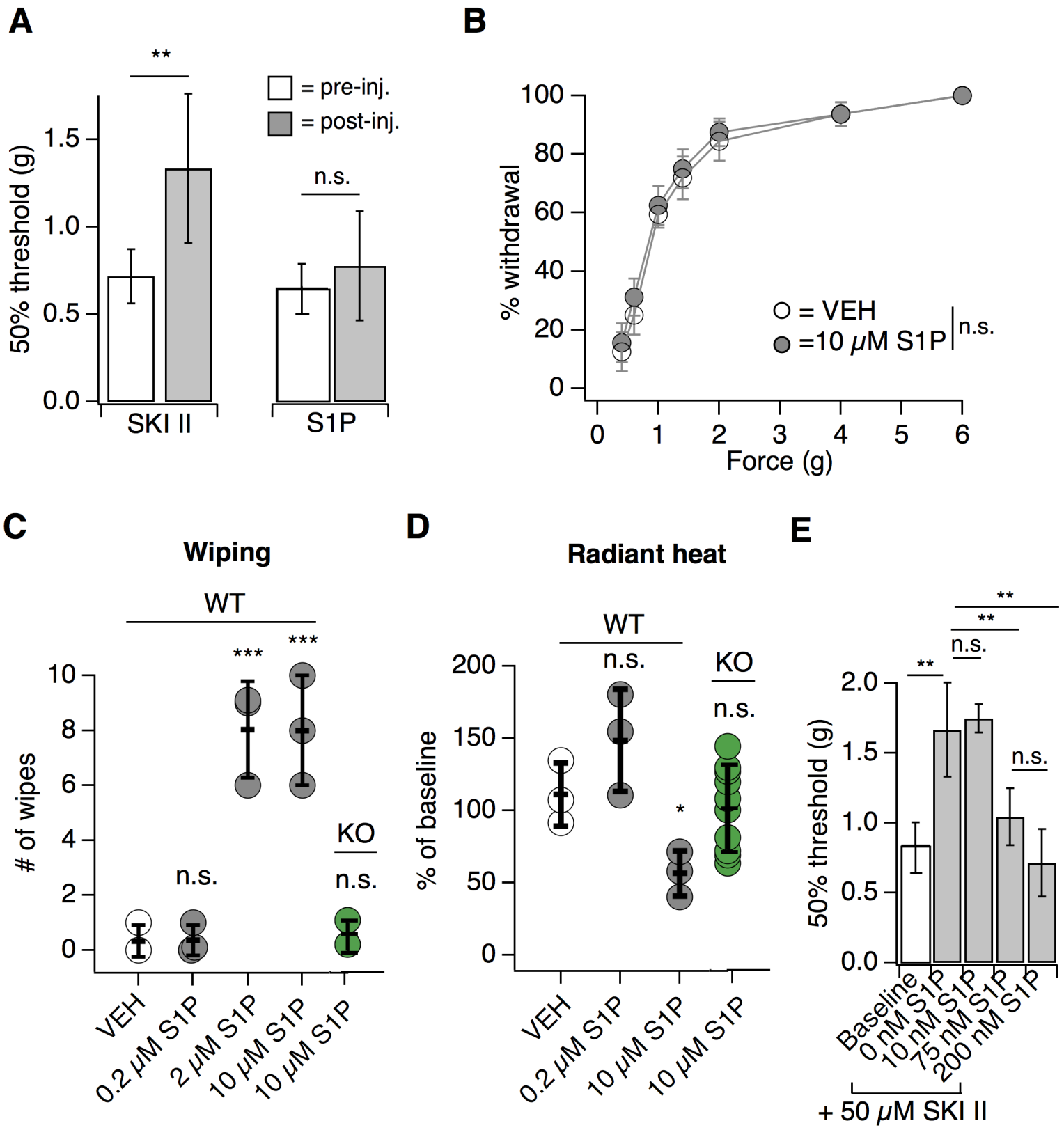
A
**
= pre-inj.
= post-inj.
n.s.
50% threshold (g)
1.5
1.0
0.5
0.0
SKI II
S1P
B
100
80
60
40
20
0
% withdrawal
= VEH
=10 μM S1P
n.s.
0
1
2
3
4
5
6
Force (g)
C
Wiping
WT
***
***
10
8
6
4
2
0
# of wipes
n.s.
KO
n.s.
VEH
0.2 μM S1P
2 μM S1P
10 μM S1P
10 μM S1P
D
Radiant heat
WT
n.s.
KO
n.s.
200
150
100
50
0
% of baseline
*
VEH
0.2 μM S1P
10 μM S1P
10 μM S1P
E
**
**
n.s.
**
n.s.
2.0
1.5
1.0
0.5
0.0
50% threshold (g)
Baseline
0 nM S1P
10 nM S1P
75 nM S1P
200 nM S1P
+ 50 μM SKI II

Figure 2

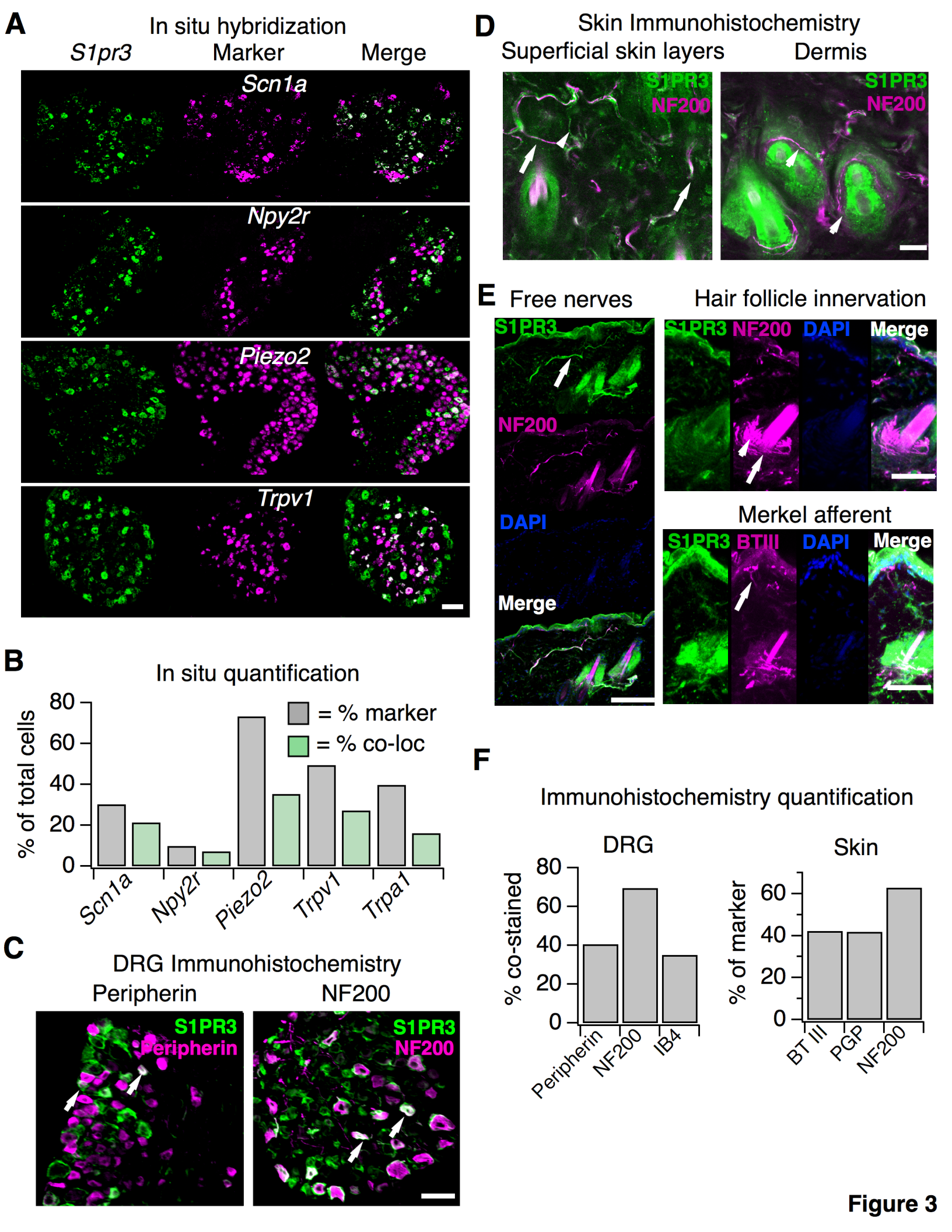
A
In situ hybridization
S1pr3
Marker
Merge
Scn1a
Npy2r
Piezo2
Trpv1
B
In situ quantification
% of total cells
80
60
40
20
0
= % marker
= % co-loc
Scn1a
Npy2r
Piezo2
Trpv1
Trpa1
C
DRG Immunohistochemistry
Peripherin
NF200
S1PR3
Peripherin
S1PR3
NF200
D
Skin Immunohistochemistry
Superficial skin layers
Dermis
S1PR3
NF200
S1PR3
NF200
E
Free nerves
S1PR3
NF200
DAPI
Merge
Hair follicle innervation
S1PR3
NF200
DAPI
Merge
Merkel afferent
S1PR3
BTIII
DAPI
Merge
F
Immunohistochemistry quantification
DRG
% co-stained
80
60
40
20
0
Peripherin
NF200
IB4
Skin
% of marker
60
40
20
0
BT III
PGP
NF200

Figure 3

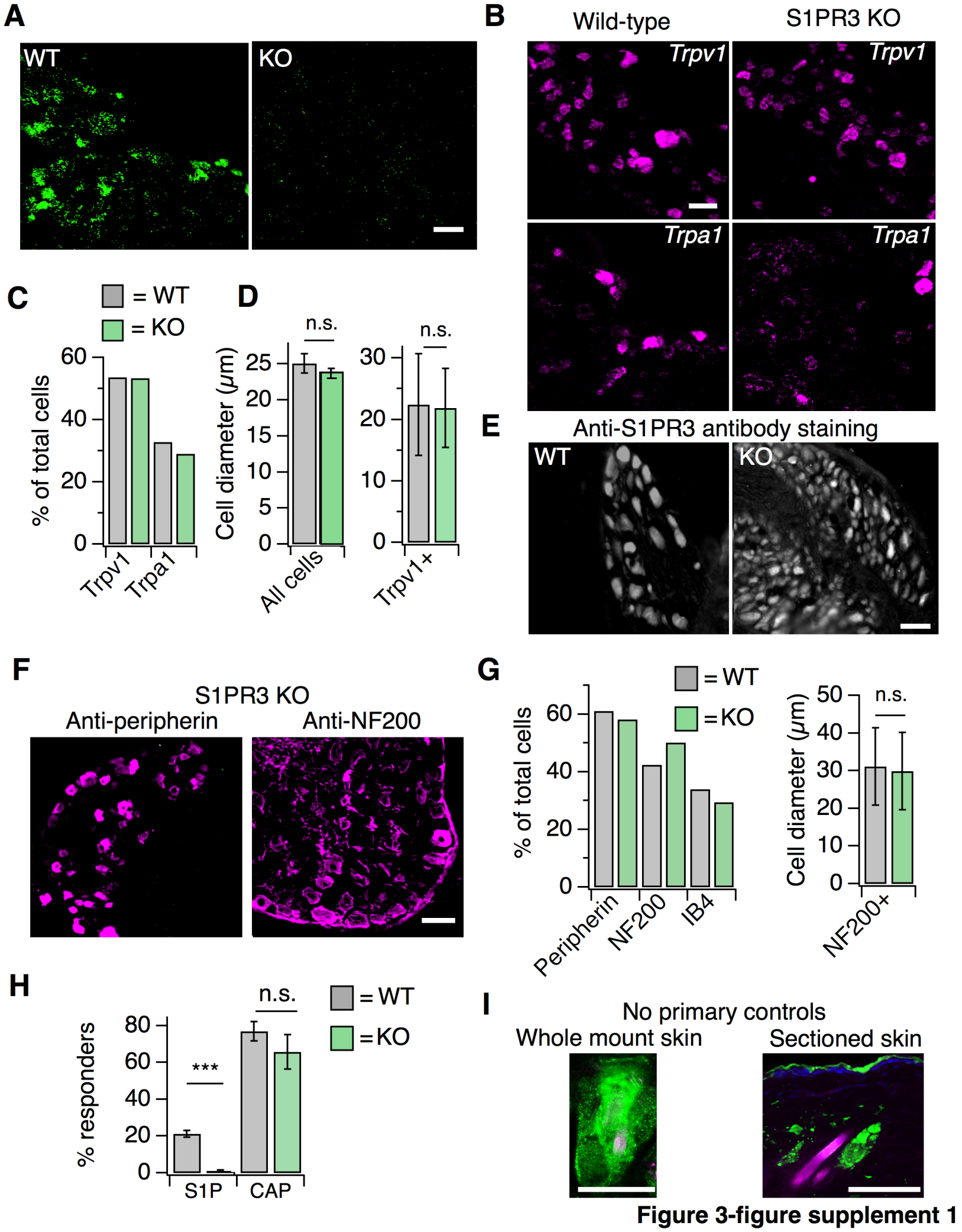

Figure 3-figure supplement 1

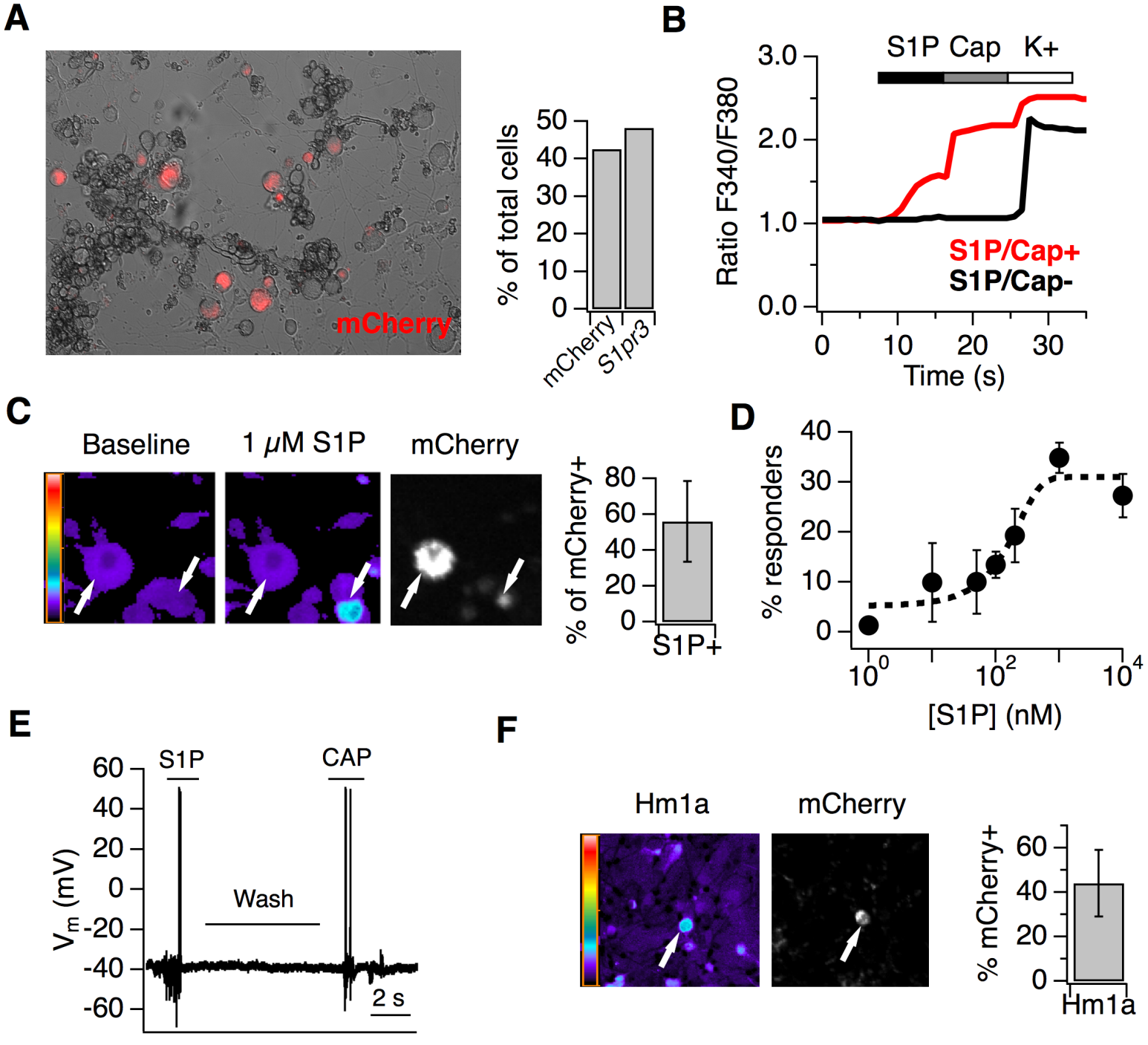
A
mCherry
% of total cells
50
40
30
20
10
0
mCherry
S1pr3
B
S1P Cap K+
Ratio F340/F380
3.0
2.0
1.0
0.0
S1P/Cap+
S1P/Cap-
0
10
20
30
Time (s)
C
Baseline
1 μM S1P
mCherry
% of mCherry+
80
60
40
20
0
S1P+
D
% responders
40
30
20
10
0
10^0
10^2
10^4
[S1P] (nM)
E
S1P
CAP
Wash
Vm (mV)
60
40
20
0
-20
-40
-60
2 s
F
Hm1a
mCherry
% mCherry+
60
40
20
0
Hm1a

Figure 4

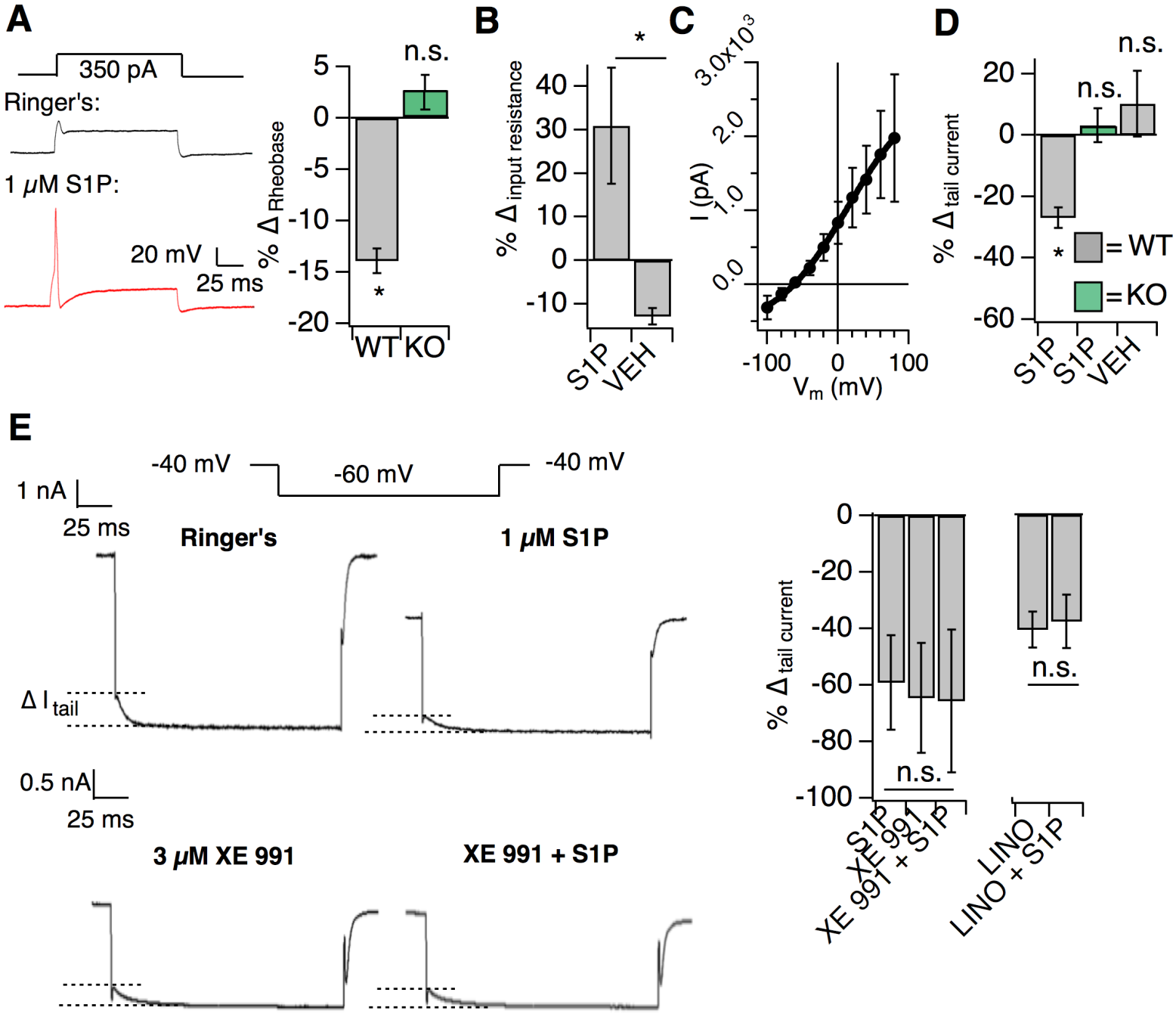
A
350 pA
Ringer's:
1 μM S1P:
20 mV
25 ms
% Δ Rheobase
n.s.
*
WT
KO
B
% Δ input resistance
*
S1P
VEH
C
I (pA)
Vm (mV)
D
% Δ tail current
n.s.
n.s.
*
= WT
= KO
S1P
S1P
VEH
E
-40 mV
-60 mV
-40 mV
1 nA
25 ms
Ringer's
1 μM S1P
Δ I tail
0.5 nA
25 ms
3 μM XE 991
XE 991 + S1P
% Δ tail current
n.s.
n.s.
S1P
XE 991
XE 991 + S1P
LINO
LINO + S1P

Figure 5

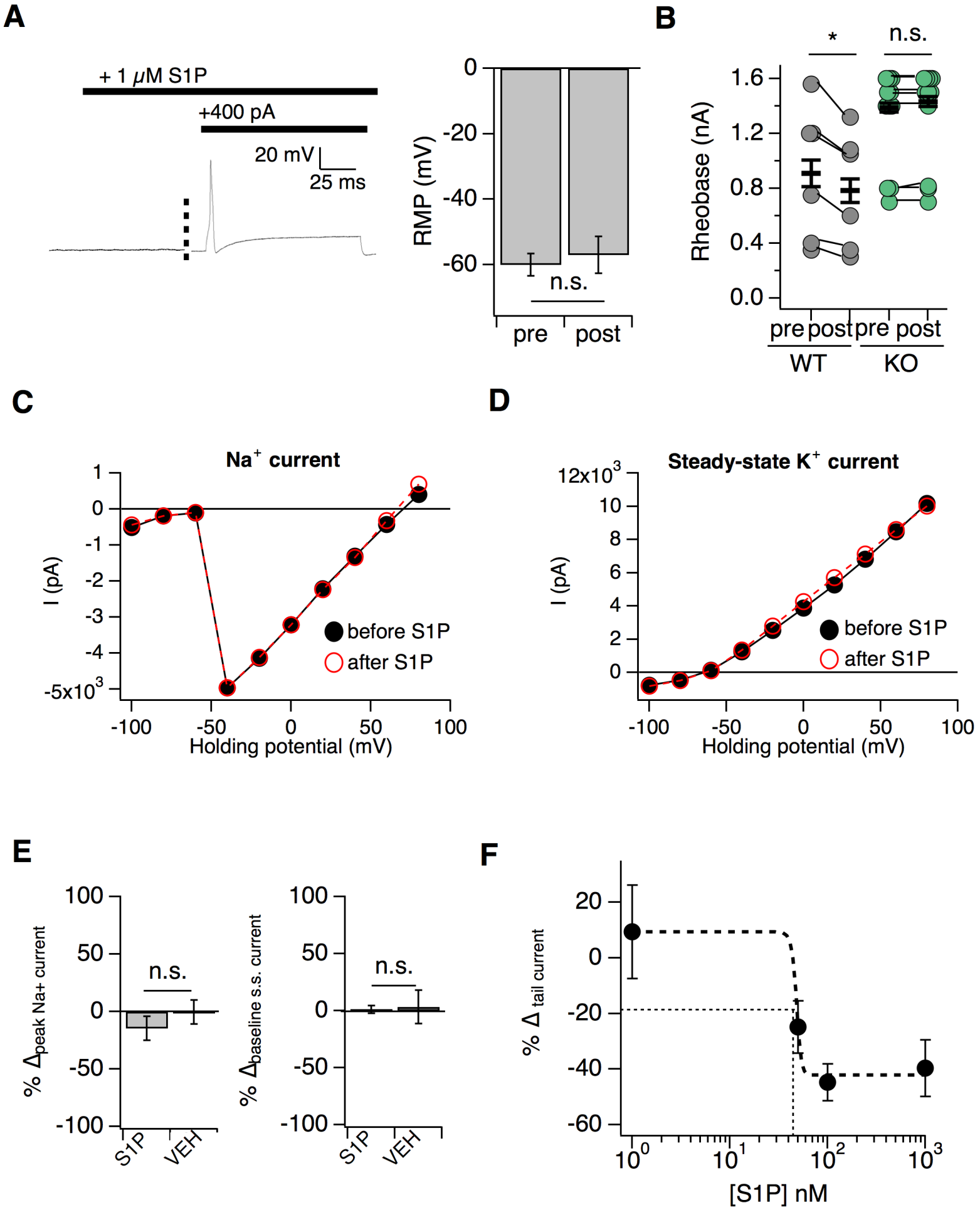

Figure 5-figure supplement 1

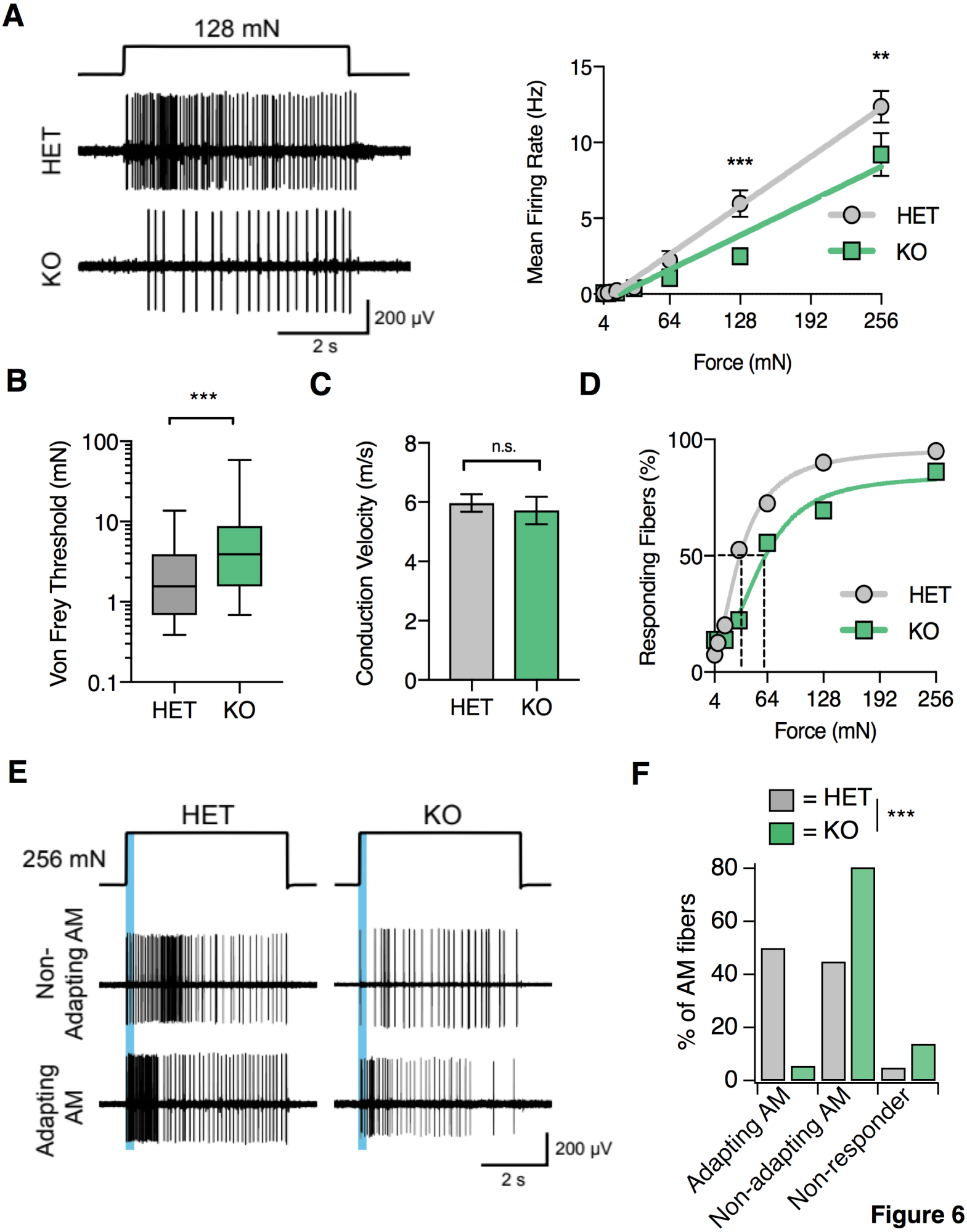
A
128 mN
HET
KO
200 µV
2 s
Mean Firing Rate (Hz)
15
10
5
0
**
***
HET
KO
4
64
128
192
256
Force (mN)
B
***
Von Frey Threshold (mN)
100
10
1
0.1
HET
KO
C
Conduction Velocity (m/s)
8
6
4
2
0
n.s.
HET
KO
D
Responding Fibers (%)
100
50
0
HET
KO
4
64
128
192
256
Force (mN)
E
HET
KO
256 mN
Non-Adapting AM
Adapting AM
200 µV
2 s
F
= HET
= KO
***
% of AM fibers
80
60
40
20
0
Adapting AM
Non-adapting AM
Non-responder

Figure 6

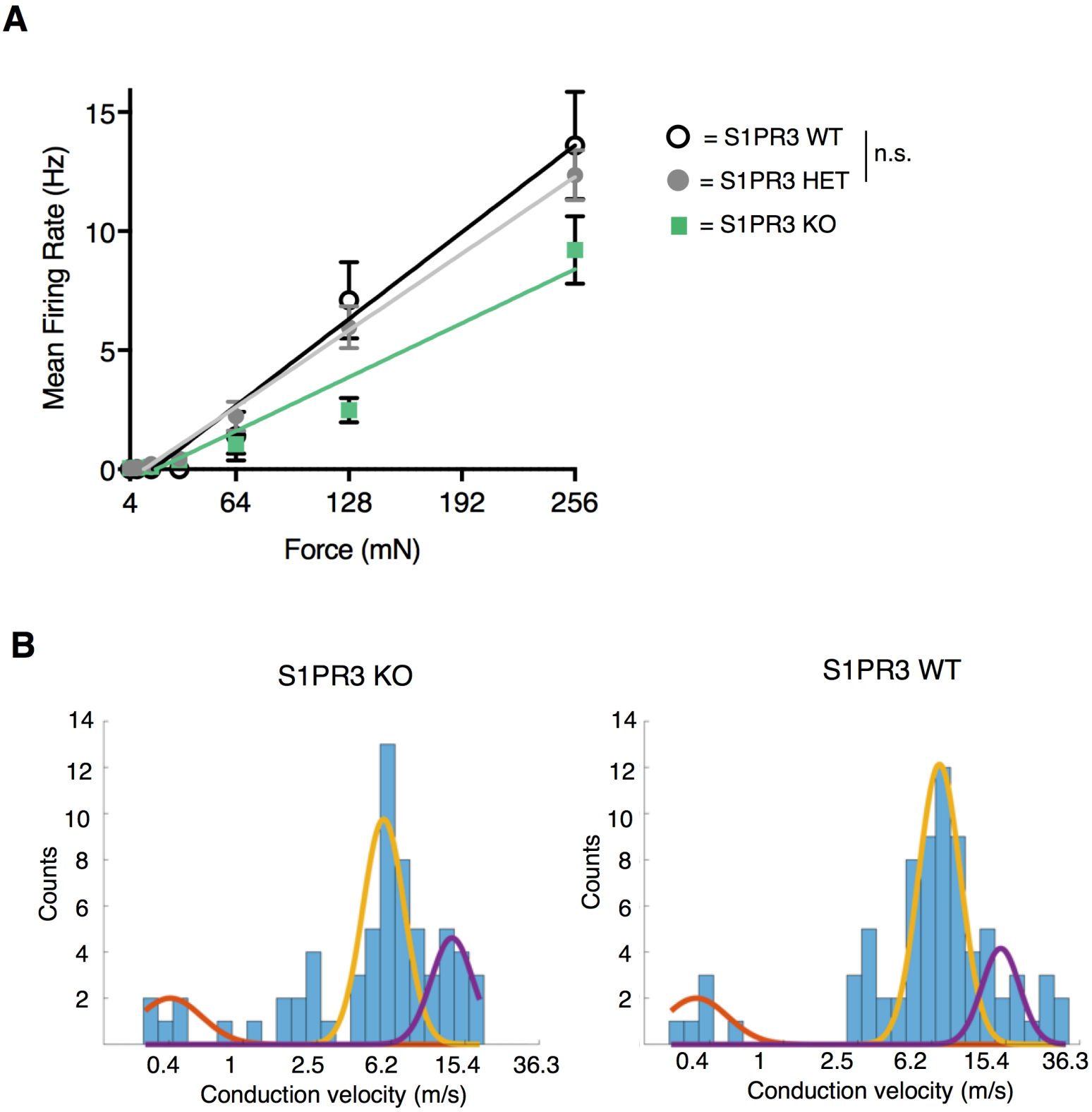

Figure 6-figure supplement 1

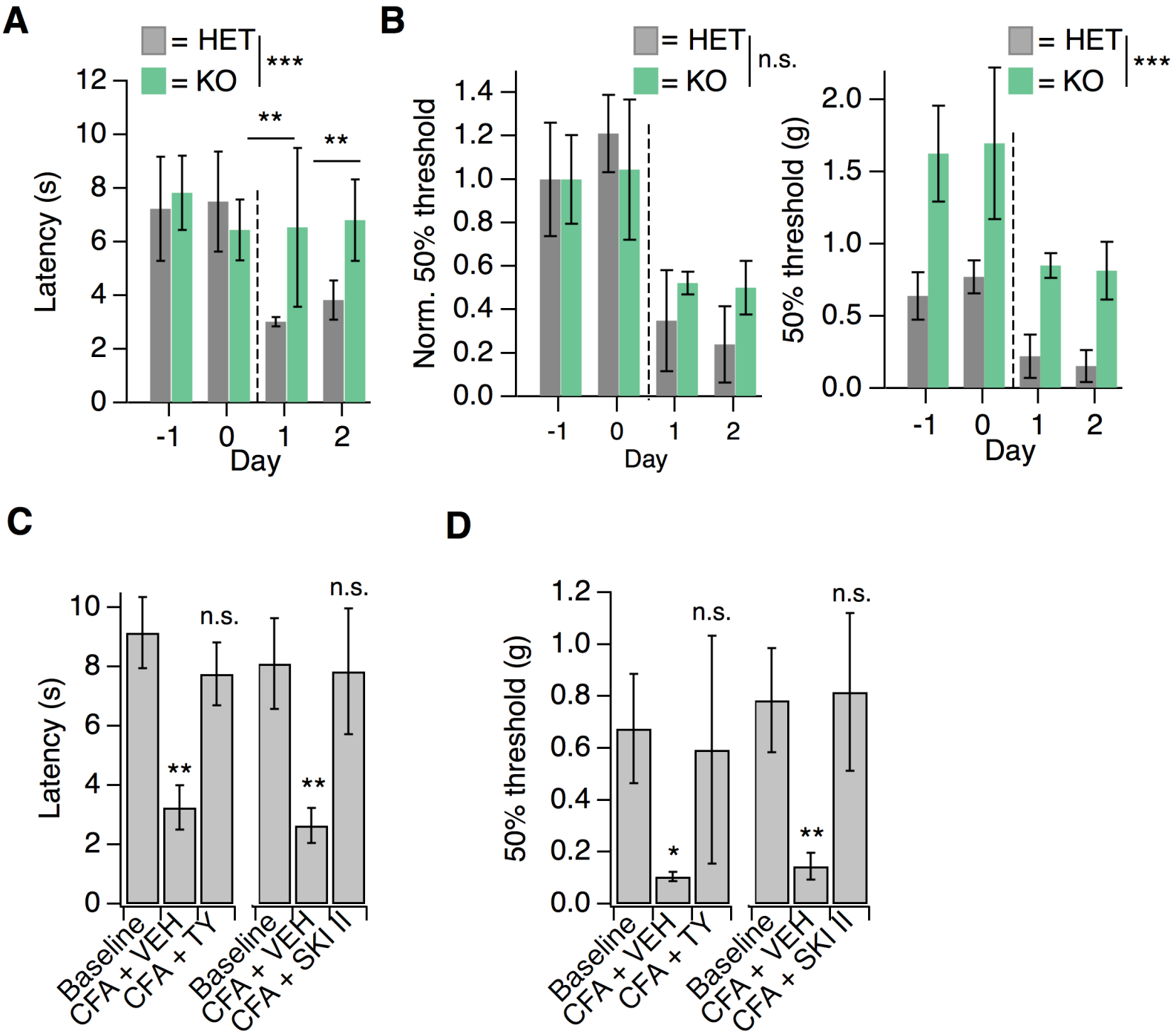
A
= HET
= KO
***
**
**
Latency (s)
Day
B
= HET
= KO
n.s.
Norm. 50% threshold
Day
= HET
= KO
***
50% threshold (g)
Day
C
Latency (s)
n.s.
n.s.
**
**
Baseline
CFA + VEH
CFA + TY
Baseline
CFA + VEH
CFA + SKI II
D
50% threshold (g)
n.s.
n.s.
*
**
Baseline
CFA + VEH
CFA + TY
Baseline
CFA + VEH
CFA + SKI II

Figure 7

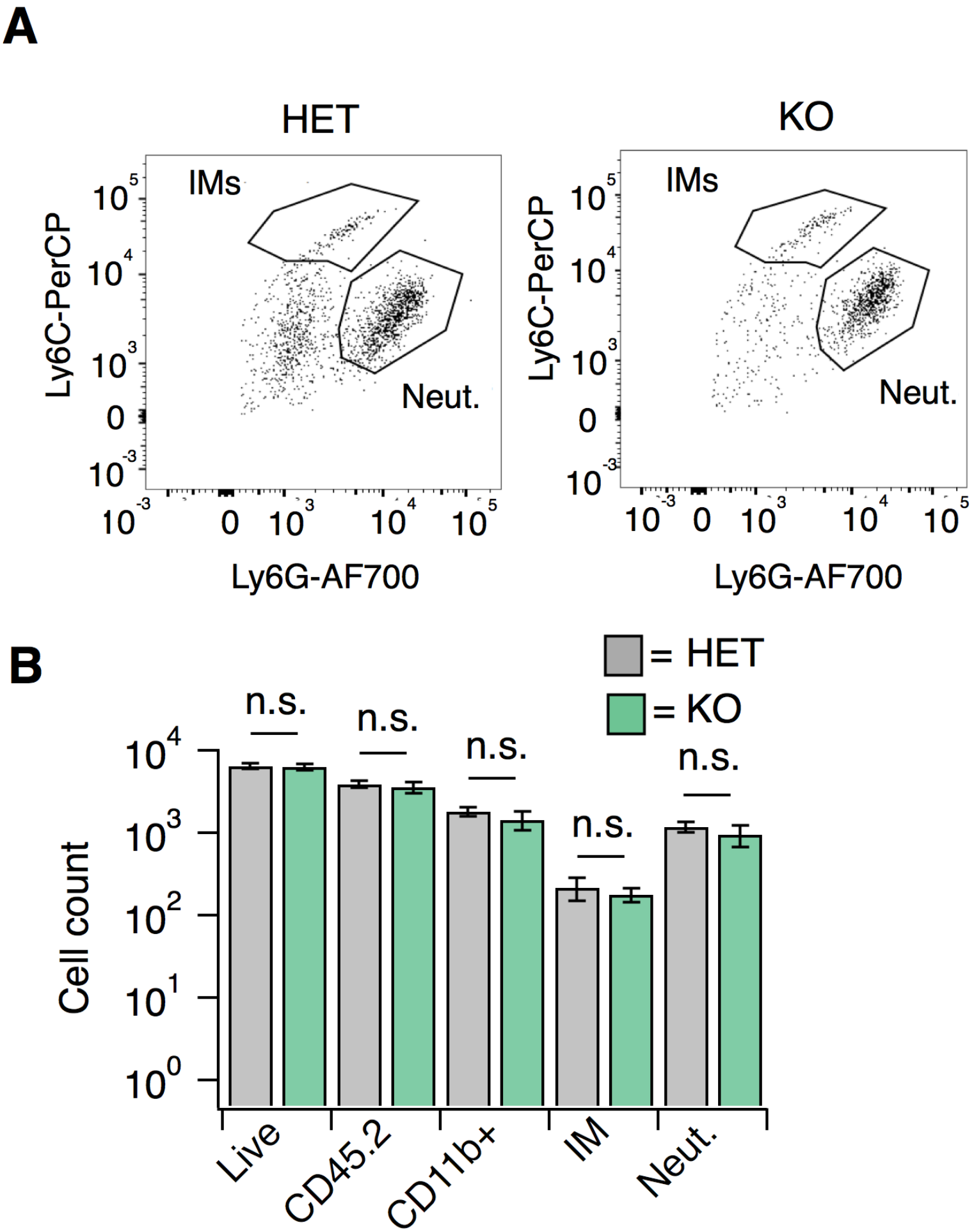

Figure 7-figure supplement 1

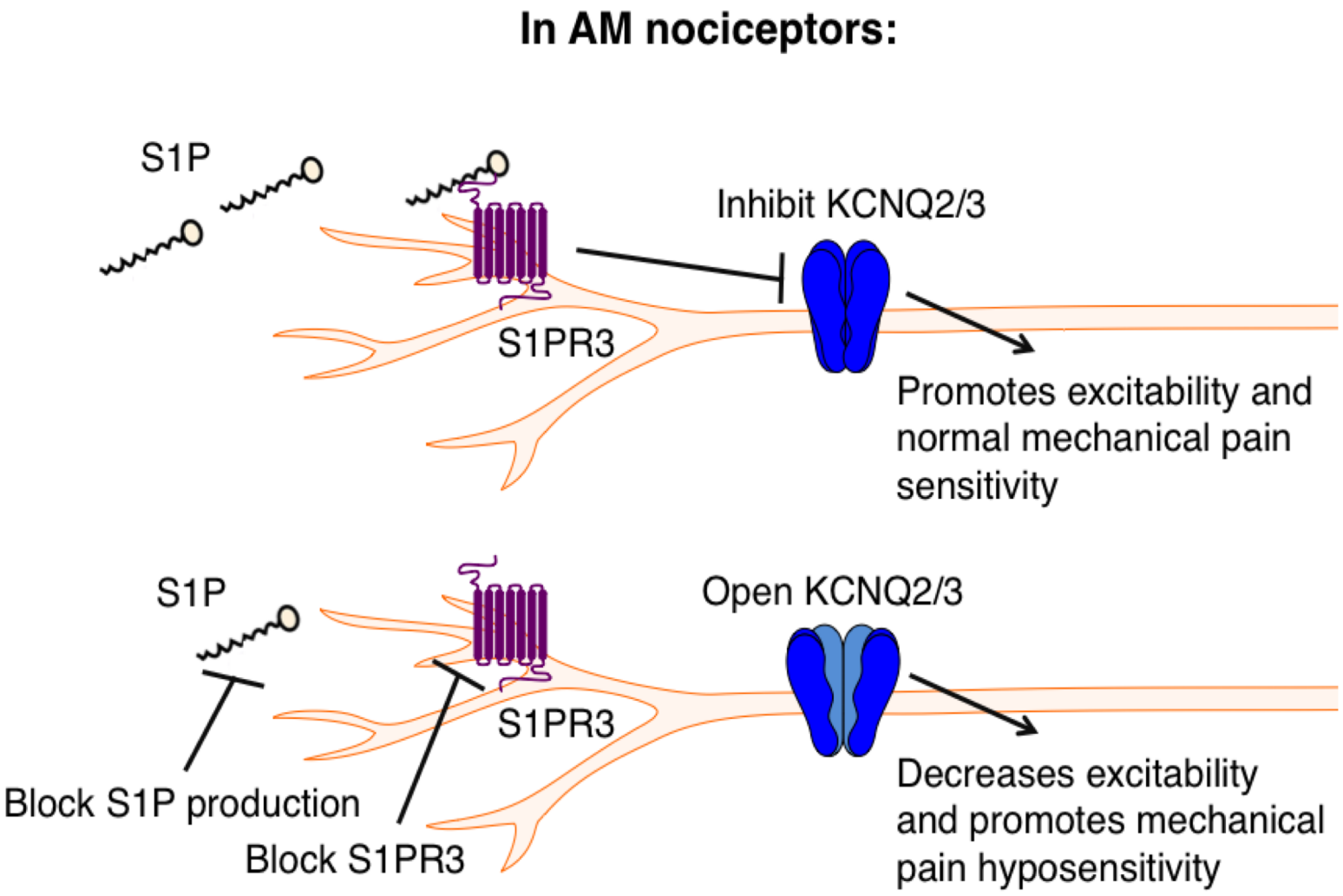
In AM nociceptors:
S1P
Inhibit KCNQ2/3
S1PR3
Promotes excitability and normal mechanical pain sensitivity
S1P
Open KCNQ2/3
S1PR3
Block S1P production
Block S1PR3
Decreases excitability and promotes mechanical pain hyposensitivity

Figure 8